

# Gravitational Lensing - Black Hole Imaging

Wouter Kleynen



Supervisor: Dr. P.M. Visser  
Advisor (committee): Dr. K.P. Hart

*Bachelor thesis for Applied Mathematics*

# Gravitational Lensing - Black Hole Imaging

Wouter Kleynen

## Abstract

A black hole is an object in space where the pull of its gravity is so strong that no light can escape. This notion gives rise to the phenomenon called gravitational lensing which is the effect where light is being bent by a massive object, in our case a black hole. With these two concepts in mind we are able to formulate the goal of this thesis: we aim to simulate and visualize the distortion of a projected image caused by the gravitational field of a black hole.

First of all we need to cover the relevant Physics to form some sort of understanding of the bigger picture and have an idea of all the factors involved in reaching that goal. We are then able to create a concrete plan to reach our goal in manageable consecutive steps.

We find that determining geodesics in a specified metric is one of the most important factors of this plan. In order to do so we derive the geodesic equation which enables us to calculate these geodesics.

We continue by first applying the geodesic equation in two-dimensional Euclidean space. This provides us with a system of differential equation which we solve by means of numerical methods. These results are visualised and proved to be correct.

We then move over to four-dimensional Minkowski space where we calculated and visualised the geodesics for this specific metric. In the Minkowski space we make a start with actually visualizing the paths of light rays.

We continue to our final metric, the Schwarzschild metric. The Schwarzschild geometry essentially describes the spacetime geometry of empty space surrounding any spherical mass which in our case will be a black hole. We calculate and visualize the geodesics thoroughly and created the image constructor for the Schwarzschild metric. This image constructor visualises how an image will be altered by being projected in a Schwarzschild metric with respect to that image in the Minkowski metric. Once the image constructor is up and running a significant amount of time is specifically dedicated to showcasing the constructed images.

We conclude that we have reached our defined goal since we are able to simulate and construct the projected images. We look back at all the steps

that played a key role in this process.

Besides the goal, we spent some time reflecting at all the unfamiliar Physics and Mathematical theory that had to be understood and applied in order to create the entire thesis.

# Contents

<b>1</b>	<b>Introduction</b>	<b>5</b>
<b>2</b>	<b>Crash course necessary physics</b>	<b>6</b>
<b>3</b>	<b>Approach to reach our goal</b>	<b>8</b>
<b>4</b>	<b>Mathematical derivation of the geodesic equation</b>	<b>9</b>
<b>5</b>	<b>Euclidean metric</b>	<b>15</b>
5.1	Defining the metric . . . . .	15
5.2	Determining the metric tensor . . . . .	16
5.3	Determining the Christoffel symbols (extrinsic approach) . . . . .	17
5.4	Metric tensor entry only Christoffel symbol formula . . . . .	18
5.5	Determining the Christoffel symbols (by intrinsic approach) . . . . .	20
5.6	Deriving the system of differential equations . . . . .	21
5.7	Solving the system of differential equations . . . . .	22
<b>6</b>	<b>Minkowski metric</b>	<b>26</b>
6.1	Defining the metric . . . . .	26
6.2	Determining the metric tensor . . . . .	26
6.3	Determining the Christoffel symbols . . . . .	27
6.4	Deriving the system of differential equations . . . . .	29
6.5	Solving the system of differential equations . . . . .	30
6.6	Setting the initial condition of light rays . . . . .	33
6.7	Plotting light rays . . . . .	35
6.8	Transforming images . . . . .	37
<b>7</b>	<b>Schwarzschild metric</b>	<b>42</b>
7.1	Defining the metric . . . . .	42
7.2	Determining the metric tensor . . . . .	42
7.3	Determining the Christoffel symbols . . . . .	42
7.4	Deriving the system of differential equations . . . . .	44
7.5	Solving the system of differential equations . . . . .	45
7.6	Defining the $t$ velocity . . . . .	47
7.7	Plotting light rays . . . . .	47
7.8	Transforming images . . . . .	52
<b>8</b>	<b>Created images</b>	<b>58</b>
<b>9</b>	<b>Conclusion</b>	<b>66</b>
	<b>References</b>	<b>69</b>

# 1 Introduction

A black hole is essentially a huge amount of matter squeezed into an extremely tiny space - think of a star ten times more massive than the Sun squeezed into a sphere approximately the diameter of New York City. This creates an object in the universe where the pull of its gravity is so strong that no matter or radiation can escape, including light. There are various astronomical events that can cause the formation of black holes, and we actually know for certain that black holes exist in our universe. It may seem like black holes are eternal doom objects that will suck in and destroy anything in the universe, but that is not the case. In fact if we were to replace our sun with a black hole of the same mass the orbit of the earth would be the same and we would not be sucked in, but remain where we are. You can however imagine that the closer you get to a black hole, the greater your required velocity should be to escape its massive gravitational pull. This minimum velocity required to escape an object's gravitational pull is what's known as the escape velocity. The event horizon is the threshold around the black hole where the escape velocity surpasses the speed of light. Since nothing can travel faster than the speed of light, the event horizon forms an invisible sphere around a black hole where there is no point of return. Every piece of matter and energy will inevitably be sucked into the *singularity* - a place at the center of the black hole where matter is compressed down to an infinitely tiny point, and all conceptions of time and space completely break down. Nobody knows what happens inside of a singularity and we will most likely never find out.

Since light cannot escape from within a black hole's event horizon, it is clear that a black hole itself can not be seen. What can be seen however is how the black hole's gravitational pull affects matter and radiation around it. In order to visualise this, we take the perspective of an observer who is located in front of the black hole at a specified distance and place an image behind the black hole at equal distance. This image is being projected to the observer. As the light rays of the image move towards the observer they have to pass around (or even through) the black hole. Light rays that pass close to the black hole (within the event horizon) get caught and cannot escape. Light rays that pass a little further away do not get caught but do get bent by the black hole's gravity. This bending of light is known as *gravitational lensing*. This gravitational lensing makes the image behind the black hole appear distorted to the observer in front of the black hole. This distortion of the image caused by the gravitational field of a black hole is exactly what we aim to simulate and visualise and therefore forms the ultimate goal of this thesis: black hole imaging.

Before we continue, I would like to thank Dr. P.M. Visser personally. Specifically for guiding me through the entire process and helping me with each and every problem I was struggling with. His help contributed to all the achieved results.

## 2 Crash course necessary physics

While researching for and working on my thesis, I had to deal with an overwhelming amount of new material. That is because the foundation of my topic is based almost solely on pure Physics. Since I have elementary knowledge of Physics, none of these concepts that formed this foundation appeared familiar to me in any way whatsoever. I found that in order to make sense of it all, it was most useful to have a more applied, theoretical, perhaps intuitive understanding of the required physics involved rather than trying to fully grasp the exact definitions, formulas, theorems and their corresponding derivations. Therefore I dedicated this section to clarify some crucial concepts on a general level, which will prove to be very important throughout the thesis.

We start all the way back in 1687, in this year Newton published his theory of gravity [8]. Newton's laws of physics described the motion of massive objects, like planets and stars. His theory stated that the three-dimensional geometry of the universe was independent of one-dimensional time. In Newton's universe, space was flat. Space was a stationary entity, which can be seen as a Cartesian grid: a three dimensional structure with an  $x$ ,  $y$  and  $z$  axis. In this Euclidean space, distance is defined by means of the three-dimensional Pythagoras theorem. This definition of distance within a specified space is what's called a *metric*. Formally a metric is a function that provides a distance value between each pair of point elements of a set.

Newtons theory proposed that time passed at the same rate no matter your frame of reference. This means that any observer should experience space and time exactly the same as one another. It took till the end of the 19th century to prove that Newton's conception was flawed. It turned out that particles that moved close to the speed of light, actually had a different experience of time (it dilates) and space (it contracts) with respect to a particle that was either slow-moving or at rest. A particle's energy or momentum was frame-dependent, which means that space and time were not absolute quantities like Newton predicted. The way anyone experienced the universe was dependent on their own motion through it. This renewed interpretation of the laws that govern the universe all derived from Albert Einstein's work. Einsteins theory that overthrew Newton's theory is what is known as *special relativity* and It is based on two postulates [9]:

- The laws of physics are invariant (i.e., identical) in all inertial systems (i.e., non-accelerating frames of reference).
- The speed of light in a vacuum is the same for all observers, regardless of the motion of the light source.

Many counter-intuitive consequences emerge when these two postulates are taken into account. For instance, the distances of pairs of events change when measured in different inertial frames of reference, and the linear additivity of velocities, as we are used to here on earth, no longer holds.

In 1908, Hermann Minkowski—once one of the math professors of a young Einstein—published a geometric interpretation of special relativity which fused time and the three dimensions of space into a single four-dimensional space now known as *Minkowski space*. Minkowski had developed the formalism of *spacetime*. Spacetime is any mathematical model which combines the three dimensions of space and the one dimension of time into a single four-dimensional *manifold* - a continuous geometrical structure having finite dimension: a line, a curve, a plane, a surface, a sphere, a ball, a cylinder, etc. Minkowski spacetime provided a space for objects to move through the universe and interact with one another. The only problem was that this space did not include gravity. If there were no such thing as the gravitational force, Minkowski spacetime would do everything we need. Spacetime would be simple and uncurved. In our universe we clearly do have the gravitational force, so Minkowski space doesn't suffice. Nonetheless, Minkowski's geometric space was to prove crucial to Einstein's development of his *general theory of relativity*. The general theory of relativity is a major building block of modern physics. It explains gravity based on the way space can 'curve', or, to put it more accurately, it associates the force of gravity with the changing geometry of spacetime. As you can imagine a black hole is a prime example of an object that performs massive space curvature. The major difference between special relativity's Minkowski space and general relativity's curved space is the mathematical formalism known as the *metric tensor*. Conceptually, the metric tensor mathematically defines how spacetime itself is curved in a given space. The matter and energy contents of that space determines the degree of spacetime curvature. As space is being curved it becomes rather difficult to define what a 'straight' path is. It may seem obvious that like in non-curved space, an object in motion will continue in this motion: Newton's first law. We visualise this as a straight line, but what curved space tells us is that an object in motion continuing in motion follows a *geodesic* and not a straight line. As a matter of fact it can be possible that a straight line as we know it is not defined in curved space at all. A geodesic can be interpreted as the shortest or straightest possible path that connects two specified points on a certain manifold. It may seem weird at first that the shortest path on particular manifolds can actually be visually apparent curved lines, but remember that since we are dealing with curved space our intuition is not that reliable anymore.

We know that the gravitational force causes spacetime curvature and that the Minkowski metric did not include this gravitational force. This means that we have no metric that implements curved spacetime. This was a problem and Physicists were looking for a metric that did. Not long after Einstein published his work on general relativity, Karl Schwarzschild found that suitable metric which is known as the *Schwarzschild metric* [10]. The Schwarzschild geometry essentially describes the spacetime geometry of empty space surrounding any spherical mass which in our case will be a black hole.

### 3 Approach to reach our goal

In the previous section (2) we briefly stated the notion of a geodesic. It will become apparent that the importance of the geodesics can't be understated throughout this thesis. That is because light is one of these entities that doesn't travel in straight lines like we are used to, but instead gets bend around massive objects like stars or black holes and thus follows a geodesic. This means that light travelling in curved space is being bent itself. Remember that our end-goal is the visualisation of an image (with respect to the observer) which is located behind the black hole which is projected to an observer in front of the black hole. If we know the exact trajectory of each light ray, starting from the original image and ending when the observer is reached, we know exactly what the image the observer perceives will look like. Simulating light rays, using an algorithm to trace the path that a ray of light would take in that specified space is known as *ray tracing*, and That is exactly what we want to do. Now, we know that a black hole curves spacetime and that light follows a geodesic in curved spacetime, so if we know how to find the specified geodesic for each light ray in this curved space, we can trace the light rays and therefore construct the image the observer perceives.

Ideally we start with the Schwarzschild metric (which describes the metric around a black hole), determine the geodesics and construct the image the observer perceives. Unfortunately this is way too much at once. Instead we start off where Physics started off as well: Newton's gravitational theory. This means we will operate in Euclidean space and determine its geodesics first: we are ray tracing in Euclidean space. This shouldn't be too much of a hassle since Euclidean space is the standard space we know all too well from Calculus and other mathematical courses. In determining the geodesics for Euclidean space we get some familiarity with all the required mathematics which will be needed for the Schwarzschild metric as well. Besides we program everything necessary to visualise the geodesics which all can be carried over to the program to visualise the Schwarzschild metric geodesics. We start of in two-dimensional Euclidean space so we can't work on the image projection yet.

We extend our Euclidean ray tracing to that of the Minkowski metric before we move on to the Schwarzschild metric. As we know Minkowski space blends the three-dimensional space and time dimension, and is basically a simplified Schwarzschild metric. we are going to determine the geodesics in Minkowski space and visualise them in a similar way as we did for the Euclidean space. In Minkowski space we can actually already start with the image projection to the observer. We trace how the light rays will move in the Minkowski space starting from the image and ending at the observer. This will lay the foundation for the Schwarzschild transformed image constructor.

Finally we move on to the Schwarzschild metric. We specify the Schwarzschild radius and determine the geodesics which allows us to reach our end-goal: visualizing the distortion of the image behind the black hole caused by the gravitational field of the black hole from the perspective of an observer in front of the black hole.

## 4 Mathematical derivation of the geodesic equation

The previous section made clear that in order to visualise the gravitational lensing of a black hole by means of ray tracing we have to be able to find the geodesics on the specified surface or manifold. It turns out there is a way to do that, by means of the *geodesic equation*. Since this equation is perhaps the most important one in this thesis, I thought it was important to determine its complete mathematical derivation so we have a good sense of what we are actually doing. This section will be dedicated to that derivation. This means however that this section is by far the most mathematical and 'abstract' section of the thesis. Nonetheless its importance can't be stated enough.

To find geodesic curves we have to define more precisely what we mean by the straightest path. A way to do this is by visualizing the geodesic curves with respect to non-geodesic curves and analyze what defines the difference between them.

In a two dimensional surface the straightest path, is the path where the acceleration vector equals zero which means the velocity is constant along the path. In a three dimensional surface or a multidimensional manifold, It is impossible to travel in a completely straight line if the embedding of the curved space in a higher-dimension Euclidean space is curved. This means that the acceleration will not be zero as is the case in the two dimensional surface. For the geodesic curve, the acceleration vectors are all present in the same plane that slices vertically through the trajectory of the path. Moreover all the acceleration vectors are normal to the surface.

It is important for our mathematical derivation that we understand the difference between tangential and normal vectors. The normal vectors of a surface are always pointing straight outwards or inwards of the surface whereas tangential vectors all lie in the plane tangent to the surface which is perpendicular to the normal vector. We are now able to formulate our specified definition of a geodesic curve. In curved space, a straight path has zero tangential acceleration when we travel along it at constant speed. We call this specific path a geodesic.

Now we are going to derive the geodesic equation by means of *extrinsic geometry*. This means that the curved space is embedded. Before we start looking for geodesic curves on surfaces It is important to note our use of space transformations. Commonly we start with the well known two dimensional  $x, y$ -plane. We put this plane through some sort of function  $\mathbf{R}$  which stretches and bends our original space such that it becomes a two dimensional surface living in three dimensional space.

$$\mathbf{R}(x, y) = (X(x, y), Y(x, y), Z(x, y))$$

We will use a parameterization with parameter  $\lambda$  to describe a curve in the original  $x, y$  plane. Then we put this curve through the function  $\mathbf{R}$  to bring it into three-dimensional space onto the surface. See the tree graph below as a clarification to all the involved variables.

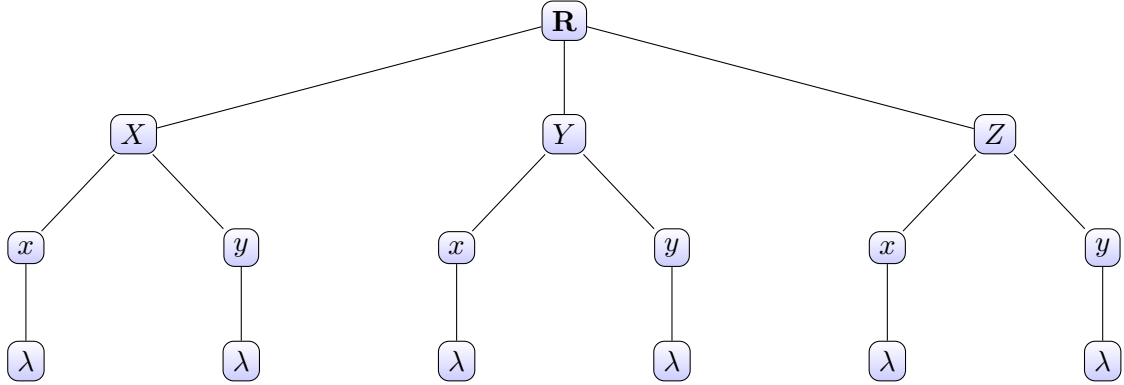


Figure 1: This tree shows how the various variables relate to each other. Each vertex connects the higher edge variable with its corresponding sub-variables in the lower connected edges.

In our search for the mathematical derivation of the geodesic equation, the length of a vector plays a crucial role. We can define the basis vectors with respect to  $x$  and  $y$  in the tangent space with  $\frac{d\mathbf{R}}{dx}$  and  $\frac{d\mathbf{R}}{dy}$  respectively. In order to know anything about the lengths of vectors, we need to know the basis vector dot-products of these derivatives. If we store these dot-products in a matrix we have what is known as the *metric tensor*. Any entry of the metric tensor of a three-dimensional space  $\mathbf{R}$  with components  $x, y$  is given by

$$g_{00} = \frac{\partial \mathbf{R}}{\partial x} \cdot \frac{\partial \mathbf{R}}{\partial x}, \quad g_{01} = \frac{\partial \mathbf{R}}{\partial x} \cdot \frac{\partial \mathbf{R}}{\partial y}, \quad g_{10} = \frac{\partial \mathbf{R}}{\partial y} \cdot \frac{\partial \mathbf{R}}{\partial x}, \quad g_{11} = \frac{\partial \mathbf{R}}{\partial y} \cdot \frac{\partial \mathbf{R}}{\partial y}$$

We briefly discussed the meaning and importance of the metric tensor in section (2) and now we are describing it mathematically. As can be seen in the expressions, above we take  $x$  to be the 'first' variable and therefore pass it index 0 denoted as  $x^0 = x$ .  $y$  is in this case the second variable and therefore has index 1 denoted as  $x^1 = y$ . This is a convention we will use throughout the thesis. This may seem unnecessary now, but in the upcoming sections we will use more variables than just  $x, y$  which means there will be more metric tensor entries, so using this convention will simplify notation. Now we are able to formulate a more general expression of our metric tensor components where  $i$  and  $j$  take on all the possible indices of the variable, and we operate in a specified space  $\mathbf{R}$ .

$$g_{ij} = \frac{\partial \mathbf{R}}{\partial x^i} \cdot \frac{\partial \mathbf{R}}{\partial x^j} \quad (1)$$

As the previous section pointed out, in order to compute geodesic curves we need to find curves where the acceleration vector is normal to the surface. The acceleration vector

will have a normal and a tangential component which can be expressed in the following way

$$\frac{d^2\mathbf{R}}{d\lambda^2} = \left(\frac{d^2\mathbf{R}}{d\lambda^2}\right)^{\text{normal}} + \left(\frac{d^2\mathbf{R}}{d\lambda^2}\right)^{\text{tangential}} \quad (2)$$

We need to find curves where the tangential component is zero so we only have a normal component. This will give us the straightest possible path between two points i.e. the geodesic. In order to do so we have to rewrite our second derivative into a pure tangential component and a pure normal component.

The tangent velocity vector along a curve can be written in terms of  $x$  and  $y$  by,

$$\frac{d\mathbf{R}}{d\lambda} = \frac{dx}{d\lambda} \frac{\partial\mathbf{R}}{\partial x} + \frac{dy}{d\lambda} \frac{\partial\mathbf{R}}{\partial y}$$

To get the acceleration vector we take the derivative of this velocity vector.

$$\begin{aligned} \frac{d}{d\lambda} \left( \frac{d\mathbf{R}}{d\lambda} \right) &= \frac{d}{d\lambda} \left( \frac{dx}{d\lambda} \frac{\partial\mathbf{R}}{\partial x} + \frac{dy}{d\lambda} \frac{\partial\mathbf{R}}{\partial y} \right) \\ &= \frac{d}{d\lambda} \left( \frac{dx}{d\lambda} \frac{\partial\mathbf{R}}{\partial x} \right) + \frac{d}{d\lambda} \left( \frac{dy}{d\lambda} \frac{\partial\mathbf{R}}{\partial y} \right) \\ &= \frac{d^2x}{d\lambda^2} \frac{\partial\mathbf{R}}{\partial x} + \frac{dx}{d\lambda} \left( \frac{d}{d\lambda} \frac{\partial\mathbf{R}}{\partial x} \right) + \frac{d^2y}{d\lambda^2} \frac{\partial\mathbf{R}}{\partial y} + \frac{dy}{d\lambda} \left( \frac{d}{d\lambda} \frac{\partial\mathbf{R}}{\partial y} \right) \end{aligned}$$

In order to further derive the expression we take a look at the expressions in parentheses. We notice that  $X, Y$  and  $Z$  are functions of  $x, y$  which at their turn are functions of  $\lambda$ . By the multi-variable chain rule we know that the  $\lambda$  derivative operator can be expanded out in a linear combination of the  $x$  and  $y$  derivative operators

$$\frac{d}{d\lambda} = \frac{dx}{d\lambda} \frac{\partial}{\partial x} + \frac{dy}{d\lambda} \frac{\partial}{\partial y}$$

So we find that,

$$\begin{aligned} \frac{d}{d\lambda} \frac{\partial\mathbf{R}}{\partial x} &= \left( \frac{dx}{d\lambda} \frac{\partial}{\partial x} + \frac{dy}{d\lambda} \frac{\partial}{\partial y} \right) \frac{\partial\mathbf{R}}{\partial x} \\ &= \frac{dx}{d\lambda} \frac{\partial^2\mathbf{R}}{\partial x^2} + \frac{dy}{d\lambda} \frac{\partial^2\mathbf{R}}{\partial x\partial y} \end{aligned}$$

And similarly,

$$\begin{aligned} \frac{d}{d\lambda} \frac{\partial\mathbf{R}}{\partial y} &= \left( \frac{dx}{d\lambda} \frac{\partial}{\partial x} + \frac{dy}{d\lambda} \frac{\partial}{\partial y} \right) \frac{\partial\mathbf{R}}{\partial y} \\ &= \frac{dx}{d\lambda} \frac{\partial^2\mathbf{R}}{\partial x\partial y} + \frac{dy}{d\lambda} \frac{\partial^2\mathbf{R}}{\partial y^2} \end{aligned}$$

Substituting this result in the expression for the acceleration vector gives

$$\begin{aligned}\frac{d}{d\lambda} \left( \frac{d\mathbf{R}}{d\lambda} \right) &= \frac{d^2x}{d\lambda^2} \frac{\partial \mathbf{R}}{\partial x} + \frac{dx}{d\lambda} \left( \frac{d}{d\lambda} \frac{\partial \mathbf{R}}{\partial x} \right) + \frac{d^2y}{d\lambda^2} \frac{\partial \mathbf{R}}{\partial y} + \frac{dy}{d\lambda} \left( \frac{d}{d\lambda} \frac{\partial \mathbf{R}}{\partial y} \right) \\ &= \frac{d^2x}{d\lambda^2} \frac{\partial \mathbf{R}}{\partial x} + \frac{dx}{d\lambda} \left( \frac{dx}{d\lambda} \frac{\partial^2 \mathbf{R}}{\partial x^2} + \frac{dy}{d\lambda} \frac{\partial^2 \mathbf{R}}{\partial x \partial y} \right) + \frac{d^2y}{d\lambda^2} \frac{\partial \mathbf{R}}{\partial y} + \frac{dy}{d\lambda} \left( \frac{dx}{d\lambda} \frac{\partial^2 \mathbf{R}}{\partial x \partial y} + \frac{dy}{d\lambda} \frac{\partial^2 \mathbf{R}}{\partial y^2} \right)\end{aligned}$$

We analyse the different types of terms we have now. We start by looking at the terms which only involve the first order derivative of  $\mathbf{R}$

$$\frac{d^2x}{d\lambda^2} \frac{\partial \mathbf{R}}{\partial x}, \quad \frac{d^2y}{d\lambda^2} \frac{\partial \mathbf{R}}{\partial y}$$

We now know that these vectors lie in the tangent plane, That is because first order derivative velocity vectors are always tangent vectors. The other four different terms do not involve first order derivatives of position vector  $\mathbf{R}$ , but second order derivatives of position vector  $\mathbf{R}$ . For now we do not know yet if these vectors lie tangent to the surface or not. We rearrange the found expression a bit so we have a clear distinction between the different types of vectors. We now have that the first two terms lie in the tangent plane and as previously mentioned, for the other vectors we do not know yet where they lie exactly. These 'leftover' terms might be tangential or normal to the surface, or even a mix of both. We are going to expand these terms in order to extract the tangential and normal components.

$$\frac{d^2\mathbf{R}}{d\lambda^2} = \frac{d^2x}{d\lambda^2} \frac{\partial \mathbf{R}}{\partial x} + \frac{d^2y}{d\lambda^2} \frac{\partial \mathbf{R}}{\partial y} + \left( \frac{dx}{d\lambda} \right)^2 \frac{\partial^2 \mathbf{R}}{\partial x^2} + \frac{dx}{d\lambda} \frac{dy}{d\lambda} \frac{\partial^2 \mathbf{R}}{\partial x \partial y} + \frac{dy}{d\lambda} \frac{dx}{d\lambda} \frac{\partial^2 \mathbf{R}}{\partial y \partial x} + \left( \frac{dy}{d\lambda} \right)^2 \frac{\partial^2 \mathbf{R}}{\partial y^2}$$

Our expression is starting to get a bit messy so we are going to apply a new form of notation. We will use what is known as *Einstein's summation convention* to simplify our expression. There are essentially three rules of Einstein's summation notation, namely:

1. Repeated indices are implicitly summed over.
2. Each index can appear at most twice in any term.
3. Each term must contain identical non-repeated indices.
  - There are two types of indices, the upper index and the lower index corresponding to two types of vectors. The upper index corresponds to the the covariant and the lower index corresponds to the contravariant.

These rules may seem a bit unclear, and the application of these rules may look a bit counter-intuitive. However after gaining some experience, the notation proves quite useful.

We set  $x^0 = x$  and  $x^1 = y$ , as we did before and apply Einstein's summation convention to arrive at the following expression

$$\frac{d^2\mathbf{R}}{d\lambda^2} = \frac{d^2x^i}{d\lambda^2} \frac{\partial \mathbf{R}}{\partial x^i} + \frac{dx^i}{d\lambda} \frac{dx^j}{d\lambda} \frac{\partial^2 \mathbf{R}}{\partial x^i \partial x^j}$$

Now as we mentioned before, the first term is in the tangent plane, but we are not sure about the second term yet. In order to find the geodesics we need to know exactly which terms are tangent, normal or a mix of both. We therefore need to thoroughly expand the term,

$$\frac{\partial^2 \mathbf{R}}{\partial x^i \partial x^j}$$

to have a better understanding of what its roll in the plane is. These second order derivatives are three dimensional vectors in in three dimensional space. This means we can expand them out as a linear combination of three dimensional basis vectors. we are choosing a different more suited basis instead of the usual  $X, Y, Z$  basis. What's different is that we are going to use the two tangent vectors  $\frac{\partial \mathbf{R}}{\partial x^0}$  and  $\frac{\partial \mathbf{R}}{\partial x^1}$  which forms our basis for the two dimensional tangent plane. Lastly for the third basis vector we are going to use a vector normal to the surface. So we rewrite our vectors in terms of our just declared three dimensional basis vectors.

We need to determine what the components of the vectors in these basis are. Since we have no further information about these components, we create new variables for these components. We are using the following notation,

$$\frac{\partial^2 \mathbf{R}}{\partial x^i \partial x^j} = \Gamma_{ij}^1 \frac{\partial \mathbf{R}}{\partial x^1} + \Gamma_{ij}^2 \frac{\partial \mathbf{R}}{\partial x^2} + L_{ij} \hat{n}$$

Here we have a division between the tangential and the normal components. The  $L_{ij}$  term is known as the second fundamental form and this represents the normal components of the second order derivative with respect to  $x^i$  and  $x^j$ . The capital gamma symbols are called the *Christoffel symbols* and these provide the tangential components of the second order derivative vector. Christoffel symbols will be one of the most important concepts in this thesis. We can group our formula more closely by applying Einstein's summation convention to the Christoffel symbols,

$$\frac{\partial^2 \mathbf{R}}{\partial x^i \partial x^j} = \Gamma_{ij}^k \frac{\partial \mathbf{R}}{\partial x^k} + L_{ij} \hat{n}$$

Now We are looking for a formula to determine our just declared Christoffel symbols. We have that  $\hat{n}$  is by definition normal to the tangent plane. That means that the dot product of  $\hat{n}$  with any of the tangent vectors is always going to be zero. We will be using this property to solve for the Christoffel symbols.

$$\frac{\partial^2 \mathbf{R}}{\partial x^i \partial x^j} \cdot \frac{\partial \mathbf{R}}{\partial x^l} = \left( \Gamma_{ij}^k \frac{\partial \mathbf{R}}{\partial x^k} + L_{ij} \hat{n} \right) \cdot \frac{\partial \mathbf{R}}{\partial x^l} = \Gamma_{ij}^k \frac{\partial \mathbf{R}}{\partial x^k} \cdot \frac{\partial \mathbf{R}}{\partial x^l} = \Gamma_{ij}^k g_{kl} \quad (3)$$

We see that the dot-product of these tangent vectors is precisely the metric tensor we defined earlier on. To isolate the Christoffel symbols we need to lose the metric tensor components. This can be done by multiply both sides of equation (3) with its inverse metric tensor.

Recall that by definition the multiplication of the metric tensor  $g_{kl}$  with its inverse  $g^{lm}$  gives us the Kronecker delta i.e

$$g_{kl}g^{lm} = \delta_k^m$$

where

$$\delta_k^m = \begin{cases} 1, & \text{if } m = k, \\ 0, & \text{if } m \neq k. \end{cases}$$

By the Kronecker delta cancellation rule we can cancel the  $k$  indices and just write the  $m$  index.

$$\frac{\partial^2 \mathbf{R}}{\partial x^i \partial x^j} \cdot \frac{\partial \mathbf{R}}{\partial x^l} g^{lm} = \Gamma_{ij}^k g_{kl} g^{lm} = \Gamma_{ij}^k \delta_k^m = \Gamma_{ij}^m \quad (4)$$

Finally we have found a formula to determine the Christoffel symbols. We can solve for the second fundamental form in a similar way, but we are not interested in these results.

We now have an equation for the acceleration vector along a curve

$$\frac{d^2 \mathbf{R}}{d\lambda^2} = \frac{d^2 x^i}{d\lambda^2} \frac{\partial \mathbf{R}}{\partial x^j} + \frac{dx^i}{d\lambda} \frac{dx^j}{d\lambda} \frac{\partial^2 \mathbf{R}}{\partial x^i \partial x^j} \quad (5)$$

where the second order derivatives are given by,

$$\frac{\partial^2 \mathbf{R}}{\partial x^i \partial x^j} = \Gamma_{ij}^k \frac{\partial \mathbf{R}}{\partial x^k} + L_{ij} \hat{n} \quad (6)$$

Substituting (6) into (5) yields,

$$\frac{d^2 \mathbf{R}}{d\lambda^2} = \frac{d^2 x^i}{d\lambda^2} \frac{\partial \mathbf{R}}{\partial x^j} + \frac{dx^i}{d\lambda} \frac{dx^j}{d\lambda} \left( \Gamma_{ij}^k \frac{\partial \mathbf{R}}{\partial x^k} + L_{ij} \hat{n} \right) \quad (7)$$

It is important to note that all the given terms in expression (7) are either given using the tangent vectors or the normal vectors. We can regroup the terms to put the normal and tangential terms separate.

$$\frac{d^2 \mathbf{R}}{d\lambda^2} = \left( \frac{d^2 x^k}{d\lambda^2} + \Gamma_{ij}^k \frac{dx^i}{d\lambda} \frac{dx^j}{d\lambda} \right) \frac{\partial \mathbf{R}}{\partial x^k} + L_{ij} \frac{dx^i}{d\lambda} \frac{dx^j}{d\lambda} \hat{n} \quad (8)$$

$$= \left( \frac{d^2 \mathbf{R}}{d\lambda^2} \right)^{\text{tangential}} + \left( \frac{d^2 \mathbf{R}}{d\lambda^2} \right)^{\text{normal}} \quad (9)$$

Now that we have performed all the required steps, we return to our initial definition of a geodesic curve. We determined that we needed to find the curves where the acceleration vector is normal to the surface. We saw in expression (2) that we could break up the acceleration vector in a tangent and normal part which is exactly what we have done in expression (8). Since we are only interested in finding the curves which are normal to the

surface we must have that the tangential part is zero and vanishes from the equation. This means that by setting the tangential part in expression (8) to zero we have an equation for finding the geodesics i.e. the geodesic equation,

$$\frac{d^2x^k}{d\lambda^2} + \Gamma_{ij}^k \frac{dx^i}{d\lambda} \frac{dx^j}{d\lambda} = 0 \quad (10)$$

We have found that any curve parameterized by  $\lambda$  which satisfies this geodesic equation given by formula (10) is a geodesic curve.

## 5 Euclidean metric

In order to have a practical understanding of the geodesic equation, It is best to start with a 'simple' or straightforward application instead of diving into the deep directly. As discussed in section (2), the common belief used to be that our universe can be seen as a three-dimensional Euclidean space, so It is sensible to start here. Actually we are taking things more slowly and start with a two-dimensional Euclidean space. This way we have a better understanding of the steps needed to be taken to solve the geodesic equation. This whole section is therefore dedicated to working with metric tensors, Christoffel symbols, coupled differential equations, etc. to prepare ourselves for the black hole metric which is to come. In addition all results are programmed in Python to form the starting blocks of the final code.

### 5.1 Defining the metric

As we know the metric associated with the two-dimensional Euclidean space is simply the Pythagoras theorem,

$$ds^2 = (dx^0)^2 + (dx^1)^2$$

Notice that we reused the upper-index notation  $x^0 = x, x^1 = y$ . We are going to transform our Cartesian plane to the sphere. In the Schwarzschild metric we deal with a spherical mass so using spherical coordinates makes everything a lot easier. We are renaming our variables  $x^0, x^1$  to compel more to the spherical notation, i.e.  $x^0 = \theta, x^1 = \phi$ . This transformation to spherical coordinates means our two-dimensional plane will be embedded in three-dimensional space given by  $(\theta, \phi) \mapsto (X(\theta, \phi), Y(\theta, \phi), Z(\theta, \phi))$ ,

$$X = r \cos(\theta) \sin(\phi)$$

$$Y = r \sin(\theta) \sin(\phi)$$

$$Z = r \cos(\theta)$$

Now our metric is redefined as the three-dimensional Pythagoras theorem.

$$ds^2 = dX^2 + dY^2 + dZ^2$$

By means of trigonometric identities the metric can be rewritten in spherical coordinates only,

$$ds^2 = dr^2 + r^2 d\theta^2 + r^2 \sin(\theta)^2 d\phi^2 \quad (11)$$

This version of the three-dimensional metric will not be used in this section, but will be of great importance in the following-up sections.

## 5.2 Determining the metric tensor

Since we are using the three-dimensional space to solve the geodesic equation living in a two-dimensional space, this is a clear example of an extrinsic approach. Essential to solving the geodesic equation is solving the corresponding Christoffel symbols. Once we know all the Christoffel symbols, the geodesic equation can be directly derived. In order to do so we first need to compute the metric tensor by means of first derivatives and their dot products as formula (1) dictates. We use the multi-variable chain rule to find expressions of these dot-products.

$$\begin{aligned} \frac{\partial \mathbf{R}}{\partial \theta} &= \frac{\partial \mathbf{R}}{\partial X} \frac{\partial X}{\partial \theta} + \frac{\partial \mathbf{R}}{\partial Y} \frac{\partial Y}{\partial \theta} + \frac{\partial \mathbf{R}}{\partial Z} \frac{\partial Z}{\partial \theta} \\ \frac{\partial \mathbf{R}}{\partial \phi} &= \frac{\partial \mathbf{R}}{\partial X} \frac{\partial X}{\partial \phi} + \frac{\partial \mathbf{R}}{\partial Y} \frac{\partial Y}{\partial \phi} + \frac{\partial \mathbf{R}}{\partial Z} \frac{\partial Z}{\partial \phi} \end{aligned}$$

Substitution of the derivatives of the spherical coordinates gives

$$\begin{aligned} \frac{\partial \mathbf{R}}{\partial \theta} &= \frac{\partial \mathbf{R}}{\partial X} \cos(\theta) \cos(\phi) + \frac{\partial \mathbf{R}}{\partial Y} \sin(\phi) \cos(\theta) + \frac{\partial \mathbf{R}}{\partial Z} \sin(\theta) \\ \frac{\partial \mathbf{R}}{\partial \phi} &= \frac{\partial \mathbf{R}}{\partial X} \sin(\phi) \sin(\theta) + \frac{\partial \mathbf{R}}{\partial Y} \cos(\phi) \sin(\theta) \end{aligned}$$

We will use the fact that the basis vectors are orthonormal meaning that any dot product with different basis vectors equals zero and any dot product with the same basis vectors equals one. Now we determine expressions for the dot products of the first derivatives (we omit the extensive calculations by means of trigonometric identities).

$$\begin{aligned} \frac{\partial \mathbf{R}}{\partial \theta} \cdot \frac{\partial \mathbf{R}}{\partial \theta} &= r^2, & \frac{\partial \mathbf{R}}{\partial \theta} \cdot \frac{\partial \mathbf{R}}{\partial \phi} &= 0 \\ \frac{\partial \mathbf{R}}{\partial \phi} \cdot \frac{\partial \mathbf{R}}{\partial \theta} &= 0, & \frac{\partial \mathbf{R}}{\partial \phi} \cdot \frac{\partial \mathbf{R}}{\partial \phi} &= r^2 \sin(\theta)^2 \end{aligned}$$

We are able to construct the metric tensor from these dot products.

$$g_{ij} = \begin{bmatrix} \frac{d\mathbf{R}}{d\theta} \cdot \frac{d\mathbf{R}}{d\theta} & \frac{d\mathbf{R}}{d\theta} \cdot \frac{d\mathbf{R}}{d\phi} \\ \frac{d\mathbf{R}}{d\phi} \cdot \frac{d\mathbf{R}}{d\theta} & \frac{d\mathbf{R}}{d\phi} \cdot \frac{d\mathbf{R}}{d\phi} \end{bmatrix} = \begin{pmatrix} r^2 & 0 \\ 0 & r^2 \sin(\theta)^2 \end{pmatrix} \quad (12)$$

Since we are dealing with a symmetric matrix, taking the inverse of the metric tensor is simply taking the reciprocal of the expression on the diagonal.

$$g^{ij} = \begin{pmatrix} \frac{1}{r^2} & 0 \\ 0 & \frac{1}{r^2 \sin(\theta)^2} \end{pmatrix} \quad (13)$$

If we compare these results to equation (11) we see that the following holds,

$$ds^2 = g_{ij} dx^i dx^j \quad (14)$$

### 5.3 Determining the Christoffel symbols (extrinsic approach)

In the previous section we derived the metric tensor and its inverse given the spherical coordinate system. Now we only need to compute the second order derivatives and their dot-products to determine the Christoffel symbols as is given by formula (4).

$$\begin{aligned} \frac{\partial^2 \mathbf{R}}{\partial \theta^2} &= -\cos(\phi) \sin(\theta) \frac{\partial \mathbf{R}}{\partial X} - \sin(\phi) \sin(\theta) \frac{\partial \mathbf{R}}{\partial Y} - \cos(\theta) \frac{\partial \mathbf{R}}{\partial Z} \\ \frac{\partial^2 \mathbf{R}}{\partial \phi^2} &= -\cos(\phi) \sin(\theta) \frac{\partial \mathbf{R}}{\partial X} - \sin(\phi) \sin(\theta) \frac{\partial \mathbf{R}}{\partial Y} \\ \frac{\partial^2 \mathbf{R}}{\partial \phi \partial \theta} &= -\sin(\phi) \cos(\theta) \frac{\partial \mathbf{R}}{\partial X} + \cos(\phi) \cos(\theta) \frac{\partial \mathbf{R}}{\partial Y} \end{aligned}$$

The Christoffel symbols have indices  $i, j$  and  $k$ . Each of these go from 1 to 2. Therefore there are  $2^3 = 8$  Christoffel symbols in total. By Einstein summation's convention we have to sum over the index variable  $l$ .

$$\begin{aligned} \Gamma_{ij}^0 &= \frac{\partial^2 \mathbf{R}}{\partial x^i \partial x^j} \cdot \frac{\partial \mathbf{R}}{\partial x^l} g^{l0} = \frac{\partial^2 \mathbf{R}}{\partial x^i \partial x^j} \cdot \frac{\partial \mathbf{R}}{\partial x^0} g^{00} + \frac{\partial^2 \mathbf{R}}{\partial x^i \partial x^j} \cdot \frac{\partial \mathbf{R}}{\partial x^2} g^{01} \\ \Gamma_{ij}^1 &= \frac{\partial^2 \mathbf{R}}{\partial x^i \partial x^j} \cdot \frac{\partial \mathbf{R}}{\partial x^l} g^{l1} = \frac{\partial^2 \mathbf{R}}{\partial x^i \partial x^j} \cdot \frac{\partial \mathbf{R}}{\partial x^1} g^{01} + \frac{\partial^2 \mathbf{R}}{\partial x^i \partial x^j} \cdot \frac{\partial \mathbf{R}}{\partial x^2} g^{11} \end{aligned}$$

Now we have  $g^{01} = g^{10} = 0$  as can be seen from the metric inverse matrix given by (13). Therefore one end of the summation in the Christoffel symbols disappears. Substituting  $g^{00}$  and  $g^{11}$  gives.

$$\begin{aligned} \Gamma_{ij}^0 &= \frac{\partial^2 \mathbf{R}}{\partial u^i \partial x^j} \cdot \frac{\partial \mathbf{R}}{\partial u^1} \\ \Gamma_{ij}^1 &= \left( \frac{\partial^2 \mathbf{R}}{\partial x^i \partial x^j} \cdot \frac{\partial \mathbf{R}}{\partial x^l} \right) \frac{1}{\sin(\theta)^2} \end{aligned}$$

We already computed the first order derivatives and the second order derivatives. Now we need to determine the required dot products. Since we have 2 first derivatives and 4 second derivatives we get a total of 8 dot products. (We omit the extensive calculations. We use the well known trigonometric identities to find the final expressions.)

$$\begin{aligned} \frac{\partial \mathbf{R}}{\partial \theta} \cdot \frac{\partial^2 \mathbf{R}}{\partial \theta^2} &= 0, & \frac{\partial \mathbf{R}}{\partial \theta} \cdot \frac{\partial^2 \mathbf{R}}{\partial \phi^2} &= -\cos(\theta) \sin(\theta), & \frac{\partial \mathbf{R}}{\partial \theta} \cdot \frac{\partial^2 \mathbf{R}}{\partial v \partial \theta} &= \frac{\partial \mathbf{R}}{\partial \theta} \cdot \frac{\partial^2 \mathbf{R}}{\partial \theta \partial \phi} = 0, \\ \frac{\partial \mathbf{R}}{\partial v} \cdot \frac{\partial^2 \mathbf{R}}{\partial \theta^2} &= 0, & \frac{\partial \mathbf{R}}{\partial \phi} \cdot \frac{\partial^2 \mathbf{R}}{\partial \phi^2} &= 0, & \frac{\partial \mathbf{R}}{\partial \phi} \cdot \frac{\partial^2 \mathbf{R}}{\partial \phi \partial \theta} &= \frac{\partial \mathbf{R}}{\partial \phi} \cdot \frac{\partial^2 \mathbf{R}}{\partial \theta \partial \phi} = \cos(\theta) \sin(\theta) \end{aligned}$$

There are only 2 non-zero dot products. We rewrite them to conform to the Einstein's summation convention. We use the commutative property of the dot product.

$$\begin{aligned} \frac{\partial^2 \mathbf{R}}{\partial \phi^2} \cdot \frac{\partial \mathbf{R}}{\partial \theta} &= -\cos(\theta) \sin(\theta) = \frac{\partial^2 \mathbf{R}}{\partial \theta^2 \partial \theta^2} \cdot \frac{\partial \mathbf{R}}{\partial u^1} \\ \frac{\partial^2 \mathbf{R}}{\partial \theta \partial \phi} \cdot \frac{\partial \mathbf{R}}{\partial \phi} &= \cos(\theta) \sin(\theta) = \frac{\partial^2 \mathbf{R}}{\partial x^1 \partial x^2} \cdot \frac{\partial \mathbf{R}}{\partial u^2} \end{aligned}$$

We substitute the non-zero dot products into the Christoffel symbol formulas to find expressions for the non-zero Christoffel symbols.

$$\begin{aligned} \Gamma_{11}^0 &= \frac{\partial^2 \mathbf{R}}{\partial x^1 \partial x^1} \cdot \frac{\partial \mathbf{R}}{\partial x^0} = -\cos(\theta) \sin(\theta) \\ \Gamma_{01}^1 &= \frac{\partial^2 \mathbf{R}}{\partial x^0 \partial x^1} \cdot \frac{\partial \mathbf{R}}{\partial \theta^2 \sin(\theta)^2} = \frac{\cos(\theta) \sin(\theta)}{\sin(\theta)^2} = \frac{\cos(\theta)}{\sin(\theta)} \end{aligned}$$

The order of differentiation of second order derivatives doesn't matter. Therefore,

$$\frac{\partial^2 \mathbf{R}}{\partial x^i \partial x^j} = \frac{\partial^2 \mathbf{R}}{\partial x^j \partial x^i}$$

which implies that,

$$\Gamma_{ij}^k = \Gamma_{ji}^k$$

We use this to show there is another non-zero Christoffel symbol.

$$\Gamma_{01}^1 = \Gamma_{10}^1 = \frac{\cos(\theta)}{\sin(\theta)}$$

#### 5.4 Metric tensor entry only Christoffel symbol formula

You might wonder why this section is dedicated to determining the Christoffel symbols of our defined space if That is exactly what we already just did. In subsection (5.3) we noticed that our approach was extrinsic: our two-dimensional space is embedded in a three-dimensional space, where we use this three-dimensional space to determine our results. This method works quite well in this case but as we deal with higher dimensional spaces, we like to omit this approach. We previously determined the Christoffel symbols by means of an extrinsic approach, i.e. by the dot-products of the basis vectors. For an intrinsic approach we no longer deal with the  $X, Y, Z$  basis and therefore we can't compute the required dot-products. We therefore need a new strategy to find the Christoffel

symbols. We start by noticing that the metric tensor components are symmetric. By formula (1) and the fact that the dot-product is symmetric, we have,

$$g_{ij} = \frac{\partial}{\partial x^i} \cdot \frac{\partial}{\partial x^j} = \frac{\partial}{\partial x^j} \cdot \frac{\partial}{\partial x^i} = g_{ji}$$

The metric tensor is so crucial that we require the dot-products above to be defined. In our case we declare the metric tensor to be (12). Next we notice that since the order of differentiation doesn't matter, we have

$$\frac{\partial}{\partial x^i} \left( \frac{\partial}{\partial x^j} \right) = \frac{\partial}{\partial x^j} \left( \frac{\partial}{\partial x^i} \right) \quad (15)$$

Now we express the expression above to one that includes Christoffel symbols

$$\begin{aligned} \frac{\partial}{\partial x^i} \left( \frac{\partial}{\partial x^j} \right) &= \Gamma_{ij}^k \frac{\partial}{\partial x^k} \\ \frac{\partial}{\partial x^j} \left( \frac{\partial}{\partial x^i} \right) &= \Gamma_{ji}^k \frac{\partial}{\partial x^k} \end{aligned}$$

And by (15) we have that,

$$\Gamma_{ij}^k = \Gamma_{ji}^k \quad (16)$$

We use this to find an alternative expression for the Christoffel symbols.

$$\begin{aligned} \frac{\partial}{\partial x^k} g_{ij} &= \frac{\partial}{\partial x^k} \left( \frac{\partial}{\partial x^j} \cdot \frac{\partial}{\partial x^i} \right) = \frac{\partial}{\partial x^k} \left( \frac{\partial}{\partial x^i} \right) \cdot \frac{\partial}{\partial x^j} + \frac{\partial}{\partial x^i} \cdot \frac{\partial}{\partial x^k} \left( \frac{\partial}{\partial x^j} \right) \\ &= \left( \Gamma_{ik}^l \frac{\partial}{\partial x^l} \right) \cdot \frac{\partial}{\partial x^j} + \frac{\partial}{\partial x^i} \cdot \left( \Gamma_{jk}^l \frac{\partial}{\partial x^l} \right) = \Gamma_{ik}^l \left( \frac{\partial}{\partial x^l} \cdot \frac{\partial}{\partial x^j} \right) + \Gamma_{jk}^l \left( \frac{\partial}{\partial x^i} \cdot \frac{\partial}{\partial x^l} \right) \\ &= \Gamma_{ik}^l g_{lj} + \Gamma_{jk}^l g_{il} = \Gamma_{ik}^l g_{jl} + \Gamma_{jk}^l g_{il} \end{aligned}$$

The second equality follows from what's known as metric compatibility and the last from the fact that the Christoffel symbols are scalars and therefore can be placed out of the dot-product. We rewrite the expression twice more but now with different indices. We find,

$$\frac{\partial g_{ij}}{\partial x^k} = \Gamma_{ik}^l g_{jl} + \Gamma_{jk}^l g_{il}, \quad \frac{\partial g_{ki}}{\partial x^j} = \Gamma_{kj}^l g_{il} + \Gamma_{ij}^l g_{kl}, \quad \frac{\partial g_{jk}}{\partial x^i} = \Gamma_{ji}^l g_{kl} + \Gamma_{ki}^l g_{jl}$$

Now combining these expressions,

$$\begin{aligned} \frac{\partial g_{ij}}{\partial x^k} + \frac{\partial g_{ki}}{\partial x^j} - \frac{\partial g_{jk}}{\partial x^i} &= \Gamma_{ik}^l g_{jl} + \Gamma_{jk}^l g_{il} + \Gamma_{kj}^l g_{il} + \Gamma_{ij}^l g_{kl} - \Gamma_{ji}^l g_{kl} - \Gamma_{ki}^l g_{jl} \\ &= \Gamma_{jk}^l g_{il} + \Gamma_{kj}^l g_{il} \\ &= 2\Gamma_{kj}^l g_{il} \end{aligned}$$

We multiply both with the inverse metric tensor,

$$2\Gamma_{kj}^l g_{il} g^{im} = g^{im} \left( \frac{\partial g_{ij}}{\partial x^k} + \frac{\partial g_{ki}}{\partial x^j} - \frac{\partial g_{jk}}{\partial x^i} \right)$$

Notice that that a metric tensor entry multiplied with a metric tensor inverse entry will result into the Kronicker delta, i.e.

$$\Gamma_{kj}^l \delta_l^m = \frac{1}{2} g^{im} \left( \frac{\partial g_{ij}}{\partial x^k} + \frac{\partial g_{ki}}{\partial x^j} - \frac{\partial g_{jk}}{\partial x^i} \right)$$

By the Kronicker delta cancellation rule we have,

$$\Gamma_{kj}^m = \frac{1}{2} g^{im} \left( \frac{\partial g_{ij}}{\partial x^k} + \frac{\partial g_{ki}}{\partial x^j} - \frac{\partial g_{jk}}{\partial x^i} \right) \quad (17)$$

To simplify the upcoming expressions we define,

$$g_{\alpha\mu,\nu} = \frac{\partial g_{\alpha\mu}}{\partial x^\nu} \quad (18)$$

This new formula for the Christoffel symbols is extremely powerful. Instead of using dot-products of the embedded space we only use the metric tensor entries, which we need to determine anyway. For the remainder of the thesis we will only use formula (17) to determine the Christoffel symbols. This is done by means of the intrinsic approach.

## 5.5 Determining the Christoffel symbols (by intrinsic approach)

As we saw with the extrinsic approach, we know that we have to find the eight following symbols,

$$\Gamma_{ij}^0 = \begin{pmatrix} \Gamma_{00}^0 & \Gamma_{01}^0 \\ \Gamma_{10}^0 & \Gamma_{11}^0 \end{pmatrix} \quad \Gamma_{ij}^1 = \begin{pmatrix} \Gamma_{00}^1 & \Gamma_{01}^1 \\ \Gamma_{10}^1 & \Gamma_{11}^1 \end{pmatrix}$$

Let's start by calculating the four symbols with  $\theta$  as upper index. We can write,

$$\Gamma_{ij}^0 = \frac{1}{2} g^{0\alpha} (g_{\alpha i,j} + g_{\alpha j,i} - g_{ij,\alpha})$$

In  $g^{0\alpha}$ ,  $\alpha$  can take the values of 0 and 1. Since  $g^{01} = 0$  we replace  $\alpha$  directly by 0.

$$\Gamma_{ij}^0 = \frac{1}{2} g^{00} (g_{0i,j} + g_{0j,i} - g_{ij,0}) = \frac{1}{2r^2} (g_{0i,j} + g_{0j,i} - g_{ij,0})$$

This gives us the following Christoffel symbols.

$$\begin{aligned} \Gamma_{00}^0 &= \frac{1}{2r^2} (g_{00,0} + g_{00,0} - g_{00,0}) = 0 \\ \Gamma_{01}^0 &= \frac{1}{2r^2} (g_{00,1} + g_{01,0} - g_{01,0}) = 0 \\ \Gamma_{10}^0 &= \frac{1}{2r^2} (g_{01,0} + g_{00,1} - g_{10,0}) = 0 \\ \Gamma_{11}^0 &= \frac{1}{2r^2} (g_{01,1} + g_{01,1} - g_{11,0}) = -\sin(u) \cos(u) \end{aligned}$$

These results are presented in the following matrix.

$$\Gamma_{ij}^0 = \begin{pmatrix} 0 & 0 \\ 0 & -\sin(u) \cos(u) \end{pmatrix}$$

Now we calculate the four symbols with  $\phi$  as upper index. We can write,

$$\Gamma_{ij}^1 = \frac{1}{2} g^{1\alpha} (g_{\alpha i, j} + g_{\alpha j, i} - g_{ij, \alpha})$$

In  $g^{1\alpha}$ ,  $\alpha$  can take the values of 0 and 1. Since  $g^{11} = 0$  we replace  $\alpha$  directly by 1.

$$\Gamma_{ij}^1 = \frac{1}{2} g^{11} (g_{1i, j} + g_{1j, i} - g_{ij, 1}) = \frac{1}{2r^2 \sin(u)^2} (g_{1i, j} + g_{0j, i} - g_{ij, 1})$$

This gives us the following Christoffel symbols.

$$\begin{aligned} \Gamma_{11}^1 &= \frac{1}{2r^2 \sin(u)^2} (g_{11, 1} + g_{11, 1} - g_{11, 1}) = 0 \\ \Gamma_{01}^1 &= \Gamma_{10}^1 = \frac{1}{2r^2 \sin(u)^2} (g_{00, 1} + g_{01, 0} - g_{01, 0}) = \frac{\cos(u)}{\sin(u)} \\ \Gamma_{00}^1 &= \frac{1}{2r^2 \sin(u)^2} (g_{10, 0} + g_{10, 0} - g_{00, 1}) = 0 \end{aligned}$$

These results are presented in the following matrix

$$\Gamma_{ij}^1 = \begin{bmatrix} 0 & \frac{\cos(u)}{\sin(u)} \\ \frac{\cos(u)}{\sin(u)} & 0 \end{bmatrix}$$

We now have determined all Christoffel symbols by an intrinsic approach.

## 5.6 Deriving the system of differential equations

This is the first time we'll be actually using the geodesic equation itself. It seemed kind of confusion to me the first time I used it, but when you remember Einstein's summation convention it does make sense. First of all we leave out all the zero Christoffel symbols, which results in,

$$\begin{aligned} \frac{d^2 x^0}{d\lambda^2} + \Gamma_{11}^0 \frac{dx^2}{d\lambda} \frac{dx^1}{d\lambda} &= 0 \\ \frac{d^2 x^1}{d\lambda^2} + \Gamma_{12}^2 \frac{dx^0}{d\lambda} \frac{dx^1}{d\lambda} + \Gamma_{21}^2 \frac{dx^1}{d\lambda} \frac{dx^0}{d\lambda} &= \frac{d^2 x^1}{d\lambda^2} + 2\Gamma_{12}^2 \frac{dx^0}{d\lambda} \frac{dx^1}{d\lambda} = 0 \end{aligned}$$

Substitution of the values of the non-zero Christoffel symbols gives,

$$\begin{aligned} \frac{d^2 \theta}{d\lambda^2} - \cos(\theta) \sin(\theta) \frac{d\phi^2}{d\lambda} \frac{d\phi^2}{d\lambda} &= 0 \\ \frac{d^2 \phi}{d\lambda^2} + 2 \frac{\cos(\theta)}{\sin(\theta)} \frac{d\theta}{d\lambda} \frac{d\phi}{d\lambda} &= 0 \end{aligned}$$

We see that we are dealing with two non-linear coupled second order differential equations. This is rather difficult to solve, so we rewrite this system to a system of four first order differential equations. We introduce 2 new variables  $v^0$  and  $v^1$  and set these equal to the first order derivatives. This produces the following system.

$$\begin{aligned}\frac{dv^1}{d\lambda} &= \cos(\theta) \sin(\theta) (v^2)^2 \\ \frac{dv^2}{d\lambda} &= -2 \frac{\cos(\theta)}{\sin(\theta)} v^1 v^2 \\ \frac{d\theta}{d\lambda} &= v^0 \\ \frac{d\phi}{d\lambda} &= v^1\end{aligned}$$

Remember that we are using spherical coordinates which means the plane we are operating in is a sphere itself. In order to put some sort of bound on our plane we set the radius to one ( $r = 1$ ), i.e the unit sphere.

## 5.7 Solving the system of differential equations

Solving the system of differential equations allows us to determine the geodesics on the unit sphere. After struggling some time with finding an analytic solution, I tried a numerical approach instead. I quickly came across *Euler's-method*. Euler's-method is perhaps the most simple numerical method of the Runge–Kutta numerical methods - a family of iterative methods. The method requires three inputs: an initial condition for each variable in the system of differential equations, a time-step  $dt$  which determines the accuracy and finally a value  $t_{\text{end}}$  which tells the method when to stop.

I started of by programming the Euler-method myself. In order to start the iterative process, I had to define an initial condition. I decided to start at  $\theta = \phi = 1$  to keep things simple. I set the values of  $v^0$  and  $v^1$  to 1 as well, which means the velocities have a positive direction. For  $dt$  I tried various time steps. The lower the value of  $dt$ , the more accurate the solver, the longer the computation time however. I eventually found  $dt = 0.005$  to be a suitable value. Lastly I had to pick  $t_{\text{end}}$  in such a way that there is at least one full rotation on the sphere. Only then we know the exact trajectory of the geodesic, from start to end. Since we are on a sphere the geodesic is periodic, so after one full rotation all higher  $t$  values will produce 'the same' result (perhaps some slight mismatches due to the limit in accuracy).

The Python program will return a list of  $\theta, \phi, v^0$  and  $v^1$  values which allows us to visually construct the geodesics. For starters, we are interested in how  $\phi$  relates to  $\theta$  as time progresses.

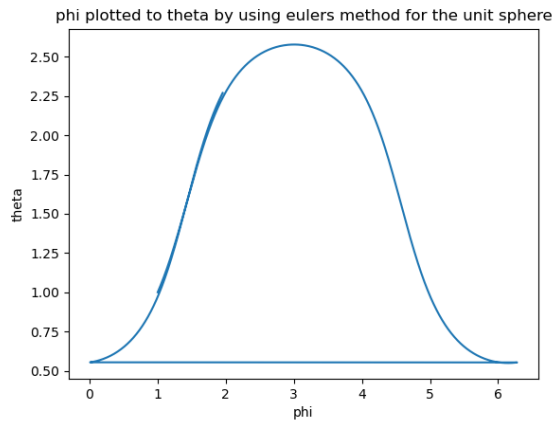


Figure 2: The trajectory of  $\phi$  with respect to  $\theta$  of the geodesic on the sphere (with initial condition set to  $(1,1,1,1)$ ), using Euler's-method.

We have limited  $\phi$  only to the interval  $[0, 2\pi]$ , since the geodesic is periodic. We see that both  $\phi$  and  $\theta$  start at 1 as prescribed, and that after a full rotation  $\phi$  and  $\theta$  return to 1 to start over again. There is a slight mismatch between the initial rotation and start of the second rotation due to the limited accuracy of Euler's-method. Decreasing  $dt$  will smooth out this gap, but will also increase computation time as previously mentioned. Notice that  $\phi$  and  $\theta$  have no linear relation so our geodesic will not be a 'straight line'. I implemented the conversion formulas from Cartesian to spherical so we are able to substitute the values for  $\phi$  and  $\theta$  into the spherical coordinates. This allows us to visualise the trajectories of  $X, Y$  and  $Z$  of the geodesic.

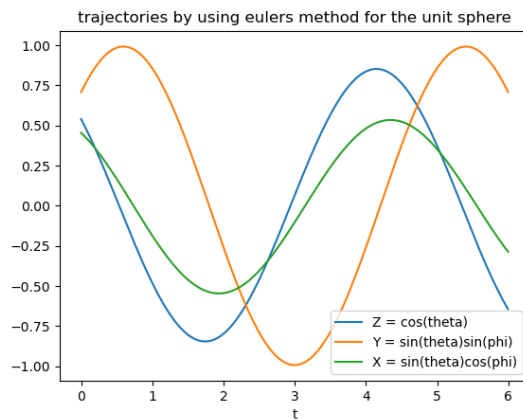


Figure 3: Geodesic trajectories in spherical coordinates (with initial condition set to  $(1,1,1,1)$ ), using Euler's-method.

We see that each trajectory is a periodic function which we expect given that we are

dealing with the unit sphere. Notice that the trajectories stop at  $t_{\text{end}} = 6$  and that the function ranges between  $-1$  and  $1$  since the radius is  $1$ .

Now that we have inspected and confirmed the Cartesian as well as the spherical trajectories we are finally able to plot the geodesic itself on the unit sphere. We use a Python three-dimensional plotter and use the lists of numerical values from the implemented Euler-method. This results into the following three dimensional plot.

geodesic plot by using eulers method for the unit sphere

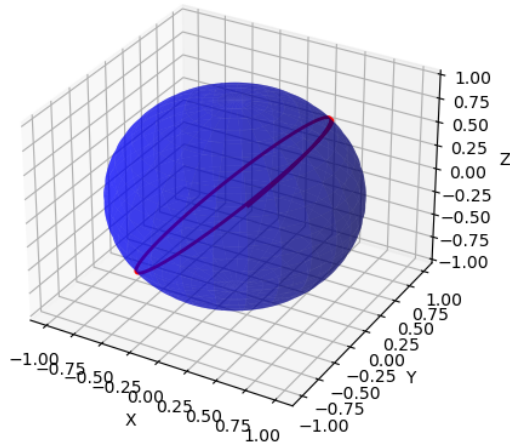


Figure 4: The three-dimensional sphere (blue) with the corresponding geodesic (red) (with initial condition set to  $(1,1,1)$ ), using Euler's-method

We can see that the geodesic on the sphere given our initial values, translates to a circle. The center of the geodesic is the center of the sphere itself. For other initial conditions, this holds as well. Therefore the geodesics are in fact all great circles. We see that there is a slight mismatch between consecutive rotations which is again due to inaccuracy of Euler's-method.

Due to the inaccuracy and relatively long computation time of the self-made Euler-method, I searched for pre-made optimized Python solvers. I found a module *odeint* which proved better than my own method in every way and was quite easy to use. For the remainder of the thesis we will use this solver instead of the self programmed Euler-method. For the upcoming metrics I did however always programmed and ran the self-made Euler-method as well as the Python solver. That is because if the outputs were similar I knew the implementation was most likely correct which was a good check. I reran the plots from this section using the Python solver to have some sort of comparison to Euler's-method.

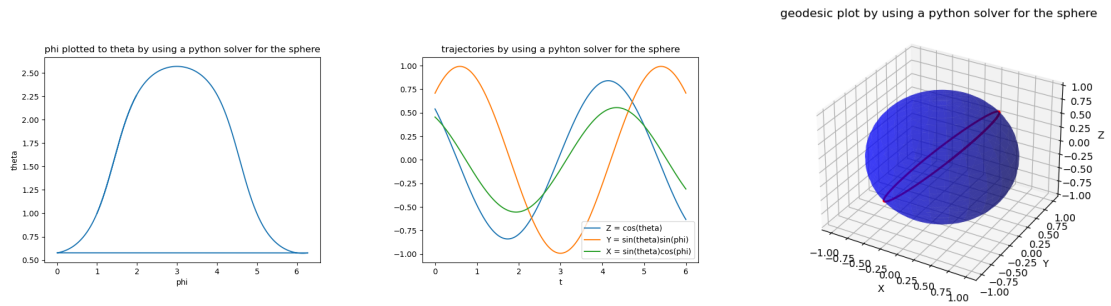


Figure 5: Generated images by means of the Python solver instead of the implemented Euler-method. Visually It is evident that the left image is more accurate in comparison to image 2 and right image is more accurate in comparison to 4.

Notice that the plots are almost identical, except for the fact that the solver plots are super smooth. Also the computation time was a lot shorter which is perhaps most important.

We are now able to construct a metric, translate a metric to the metric tensor, determine the Christoffel symbols, construct the system of first order differential equations, solve those equations and visualise the results. This approach will be applied for the upcoming metrics as well.

## 6 Minkowski metric

As mentioned in section (2) we continue with the Minkowski metric instead of going to the Schwarzschild metric directly. Even though the Euclidean metric brought us a long way, the step to the Schwarzschild metric is still too big. Therefore we prefer to delve into the Minkowski metric first since this is a sort of intermediate metric. Nonetheless the Minkowski metric actually has a lot in common with the Schwarzschild metric which proves to be very useful. We are even able to already start with image transformations at the end of this section.

### 6.1 Defining the metric

The Minkowski metric in spherical coordinates is given as,

$$ds^2 = dt^2 - dr^2 - r^2d\theta^2 - r^2(\sin\theta)^2\phi^2$$

Notice that the metric is similar to the Euclidean three-dimensional metric given by (11) we saw in the previous section. The only difference is that we have an extra component, the  $t$  variable. It is clear that we are now dealing with a four-dimensional space where time is implemented as well. Note that we will switch between  $x$  upper-index notation and spherical notation, i.e.  $x^0 = t, x^1 = r, x^2 = \theta$  and  $x^3 = \phi$ .

### 6.2 Determining the metric tensor

Unlike in subsection (5.2) where we computed the metric tensor by means of the inner dot product, we now use a different approach. We derive the metric tensor directly from the metric itself as is expressed by formula (14). The only thing we have to do is determine with which expression each variable in the metric is multiplied and substitute this expression into a diagonal matrix with each expression at its variable indexed position. We see that the indexed metric expression components are,

$$g_{00} = 1, \quad g_{11} = -1, \quad g_{22} = -r^2, \quad g_{33} = -r^2(\sin\theta)^2$$

Which gives us the Minkowski metric tensor matrix.

$$g_{ij} = \begin{pmatrix} 1 & 0 & 0 & 0 \\ 0 & -1 & 0 & 0 \\ 0 & 0 & -r^2 & 0 \\ 0 & 0 & 0 & -r^2(\sin\theta)^2 \end{pmatrix} \quad (19)$$

And its inverse, which will be needed to determine the Christoffel symbols.

$$g^{ij} = \begin{pmatrix} 1 & 0 & 0 & 0 \\ 0 & -1 & 0 & 0 \\ 0 & 0 & -\frac{1}{r^2} & 0 \\ 0 & 0 & 0 & -\frac{1}{r^2(\sin\theta)^2} \end{pmatrix} \quad (20)$$

### 6.3 Determining the Christoffel symbols

Determining the Christoffel symbols for the Minkowski space is very similar to determining the Christoffel symbols for the Schwarzschild metric. That is why this section contains quite extensive calculations, so all steps are really clear. We omit the simplified notation described in (18) to make sure all intermediate steps are understood. We use formula (17) to calculate the Christoffel symbols by means of the metric tensor only. We start by calculating the Christoffel symbols with regards to  $x^0 = t$ . Which gives,

$$\Gamma_{kj}^0 = \frac{1}{2}g^{im} \left( \frac{\partial g_{ij}}{\partial x^k} + \frac{\partial g_{ki}}{\partial x^j} - \frac{\partial g_{jk}}{\partial x^i} \right) \quad (21)$$

Since our metric tensor matrix is a 4 by four 4 we have to calculate a total of 16 Christoffel symbols for upper index 0 which can be represented in the following way

$$\Gamma_{kj}^0 = \begin{pmatrix} \Gamma_{00}^0 & \Gamma_{01}^0 & \Gamma_{02}^0 & \Gamma_{03}^0 \\ \Gamma_{10}^0 & \Gamma_{11}^0 & \Gamma_{12}^0 & \Gamma_{13}^0 \\ \Gamma_{20}^0 & \Gamma_{21}^0 & \Gamma_{22}^0 & \Gamma_{23}^0 \\ \Gamma_{30}^0 & \Gamma_{31}^0 & \Gamma_{32}^0 & \Gamma_{33}^0 \end{pmatrix}$$

We notice that in equation (21)  $i$  takes the values of 0, 1, 2, 3. Since  $g^{0i} = 0$  if  $i \neq 0$  we can replace  $i$  directly by 0.

$$\Gamma_{kj}^0 = \frac{1}{2}g^{00} \left( \frac{\partial g_{0j}}{\partial x^k} + \frac{\partial g_{0k}}{\partial x^j} - \frac{\partial g_{jk}}{\partial x^0} \right) = \frac{1}{2} \left( \frac{\partial g_{0j}}{\partial x^k} + \frac{\partial g_{0k}}{\partial x^j} - \frac{\partial g_{jk}}{\partial x^0} \right)$$

Since the variable  $x^0 = t$  does not appear in the metric tensor matrix, we have  $\frac{\partial g_{jk}}{\partial x^0} = 0$  for all  $j, k \in \{0, 1, 2, 3\}$ . Which gives us,

$$\Gamma_{jk}^1 = \frac{1}{2} \left( \frac{\partial g_{1j}}{\partial x^k} + \frac{\partial g_{1k}}{\partial x^j} \right) = 0 \quad (22)$$

Expression (22) implies that every element in the expression originates from the first row of the metric matrix, since we are left with row index  $i$  in  $g_{ij}$  equal to 1. In the metric matrix we see that the first row only has zero entries except on the diagonal, there we have a one. This means that in fact all partial derivatives of the first row with respect to any of the variables is zero so all the Christoffel symbols are zero, i.e. for all  $j, k \in \{0, 1, 2, 3\}$

$$\Gamma_{jk}^0 = \mathbf{0}$$

Now for the second variable  $x^1 = r$  we use again formula (17) to find

$$\Gamma_{jk}^1 = \frac{1}{2}g^{1i} \left( \frac{\partial g_{ij}}{\partial x^k} + \frac{\partial g_{ik}}{\partial x^j} - \frac{\partial g_{jk}}{\partial x^i} \right)$$

Here  $i$  takes the values of 0, 1, 2, 3. Since  $g^{1i} = 0$  if  $i \neq 1$  we can replace  $i$  directly by 1

$$\Gamma_{jk}^1 = \frac{1}{2}g^{11} \left( \frac{\partial g_{1j}}{\partial x^k} + \frac{\partial g_{1k}}{\partial x^j} - \frac{\partial g_{jk}}{\partial x^1} \right) = -\frac{1}{2} \left( \frac{\partial g_{1b}}{\partial x^k} + \frac{\partial g_{1k}}{\partial x^j} - \frac{\partial g_{jk}}{\partial x^1} \right) \quad (23)$$

Now for all  $j, k \in \{0, 1, 2, 3\}$  we have  $\frac{\partial g_{1j}}{\partial x^k} = 0$ . Since the second row consists of all zeros except for a -1 on the diagonal, we find that all partial derivatives of this form are zero. So we rewrite expression (23) to,

$$\Gamma_{jk}^1 = \frac{1}{2} \left( \frac{\partial g_{jk}}{\partial x^1} \right)$$

These entries are all zero again, except for the lower two diagonal entries We find,

$$\Gamma_{22}^1 = -\frac{1}{2} \left( \frac{\partial g_{22}}{\partial x^1} \right) = \frac{1}{2} (-2r) = -r$$

$$\Gamma_{33}^1 = \frac{1}{2} \left( \frac{\partial g_{33}}{\partial x^1} \right) = \frac{1}{2} (-2r(\sin(\theta))^2) = -r \sin(\theta)^2$$

Now we move on to the third variable  $x^2 = \theta$  we use again formula (17) to find

$$\Gamma_{jk}^2 = \frac{1}{2} g^{2i} \left( \frac{\partial g_{ij}}{\partial x^k} + \frac{\partial g_{ik}}{\partial x^j} - \frac{\partial g_{jk}}{\partial x^i} \right)$$

Again  $i$  takes the values of  $\{0, 1, 2, 3\}$ . Since  $g^{2i} = 0$  if  $i \neq 2$  we can replace  $i$  directly by 2.

$$\Gamma_{jk}^2 = \frac{1}{2} g^{22} \left( \frac{\partial g_{2j}}{\partial x^k} + \frac{\partial g_{2k}}{\partial x^j} - \frac{\partial g_{jk}}{\partial 2} \right) = -\frac{1}{2r^2} \left( \frac{\partial g_{2j}}{\partial x^k} + \frac{\partial g_{2k}}{\partial x^j} - \frac{\partial g_{jk}}{\partial x^2} \right) \quad (24)$$

We notice that  $\frac{\partial g_{jk}}{\partial x^2} = 0$  for all possible entries of  $j, k$  except for  $j = k = 3$  since there is a  $\theta$  term in  $g_{33}$ . So we start with this term.

$$\Gamma_{33}^2 = -\frac{1}{2r^2} \left( \frac{\partial g_{23}}{\partial x^3} + \frac{\partial g_{23}}{\partial x^3} - \frac{\partial g_{33}}{\partial x^2} \right) = \frac{-1}{2r^2} \cdot 2r^2 \sin \theta \cos \theta = -\sin \theta \cos \theta$$

Since we've calculated  $\Gamma_{33}^2$  we know that the last term vanishes for all other Christoffel symbols with 2 as upper-index so we are left with,

$$\Gamma_{jk}^2 = -\frac{1}{2r^2} \left( \frac{\partial g_{2j}}{\partial x^k} + \frac{\partial g_{2k}}{\partial x^j} \right)$$

We can take  $j = 2, k = 1$  to find

$$\Gamma_{21}^2 = -\frac{1}{2r^2} \left( \frac{\partial g_{22}}{\partial x^1} + \frac{\partial g_{21}}{\partial 2} \right) = -\frac{1}{2r^2} (-2r + 0) = \frac{1}{r}$$

We move on to the last variable:  $x^3 = \phi$ . We use again formula (17) to find,

$$\Gamma_{jk}^3 = \frac{1}{2} g^{3i} \left( \frac{\partial g_{ij}}{\partial x^k} + \frac{\partial g_{ik}}{\partial x^j} - \frac{\partial g_{jk}}{\partial x^i} \right)$$

Again  $i$  takes any of the values of  $\{0, 1, 2, 3\}$ . Since  $g^{3i} = 0$  if  $i \neq 3$  we can replace  $i$  directly by 3.

$$\Gamma_{jk}^3 = \frac{1}{2}g^{33} \left( \frac{\partial g_{3j}}{\partial x^k} + \frac{\partial g_{3k}}{\partial x^j} - \frac{\partial g_{jk}}{\partial x^3} \right) = -\frac{1}{2r^2(\sin \theta)^2} \left( \frac{\partial g_{3j}}{\partial x^k} + \frac{\partial g_{3k}}{\partial x^j} - \frac{\partial g_{jk}}{\partial x^3} \right) \quad (25)$$

Since there are no  $\phi$  entries in the metric matrix we have that  $\frac{\partial g_{jk}}{\partial x^3} = 0$  for all  $j, k$  so we leave out the last term.

$$\Gamma_{jk}^3 = -\frac{1}{2r^2(\sin \theta)^2} \left( \frac{\partial g_{3j}}{\partial x^k} + \frac{\partial g_{3k}}{\partial x^j} \right) \quad (26)$$

Take  $j = 3$  and  $k = 1$  to find a non-zero Christoffel symbol.

$$\Gamma_{31}^3 = -\frac{1}{2r^2(\sin \theta)^2} \left( \frac{\partial g_{33}}{\partial x^1} + \frac{\partial g_{31}}{\partial x^3} \right) = -\frac{1}{2r^2(\sin \theta)^2} \cdot -2r \sin(\theta)^2 = \frac{1}{r}$$

Take  $j = 2$  and  $k = 3$  to find the remaining non-zero Christoffel symbol.

$$\Gamma_{23}^3 = -\frac{1}{2r^2(\sin \theta)^2} \left( \frac{\partial g_{31}}{\partial x^3} + \frac{\partial g_{33}}{\partial x^1} \right) = -\frac{1}{2r^2(\sin \theta)^2} \cdot -2r^2 \sin(\theta) \cos(\theta) = \frac{\cos(\theta)}{\sin(\theta)}$$

By using the symmetry of the Christoffel symbols from (16) we find we find the following non-zero Christoffel symbols.

$$\begin{aligned} \Gamma_{22}^1 &= -r, & \Gamma_{33}^1 &= -r \sin(\theta)^2, & \Gamma_{21}^2 &= \Gamma_{12}^2 = \frac{1}{r} \\ \Gamma_{33}^\theta &= -\sin(\theta) \cos(\theta), & \Gamma_{31}^3 &= \Gamma_{13}^3 = \frac{1}{r}, & \Gamma_{23}^3 &= \Gamma_{32}^3 = \frac{\cos(\theta)}{\sin(\theta)} \end{aligned}$$

## 6.4 Deriving the system of differential equations

We use the formula for the geodesic equation as well as the expression for the non-zero Christoffel symbols from the previous subsection to establish the following system of differential equations (this approach is analogous to how we determined the system of differential equations in the previous section).

$$\begin{aligned} \frac{d^2 u^1}{d\lambda^2} + \Gamma_{22}^1 \frac{du^2}{d\lambda} \frac{du^2}{d\lambda} + \Gamma_{33}^1 \frac{du^3}{d\lambda} \frac{du^3}{d\lambda} &= \frac{d^2 r}{d\lambda^2} - r \frac{d\theta}{d\lambda} \frac{d\theta}{d\lambda} - r \sin(\theta)^2 \frac{d\phi}{d\lambda} \frac{d\phi}{d\lambda} = 0 \\ \frac{d^2 u^2}{d\lambda^2} + (\Gamma_{21}^2 + \Gamma_{12}^2) \frac{du^2}{d\lambda} \frac{du^1}{d\lambda} + \Gamma_{33}^2 \frac{du^3}{d\lambda} \frac{du^3}{d\lambda} &= \frac{d^2 \theta}{d\lambda^2} + \frac{2}{r} \frac{d\theta}{d\lambda} \frac{dr}{d\lambda} - \sin(\theta) \cos(\theta) \frac{d\phi}{d\lambda} \frac{d\phi}{d\lambda} = 0 \\ \frac{d^2 u^3}{d\lambda^2} + (\Gamma_{31}^3 + \Gamma_{13}^3) \frac{du^3}{d\lambda} \frac{du^1}{d\lambda} + (\Gamma_{23}^3 + \Gamma_{32}^3) \frac{du^2}{d\lambda} \frac{du^3}{d\lambda} &= \frac{d^2 \phi}{d\lambda^2} + \frac{2}{r} \frac{d\phi}{d\lambda} \frac{dr}{d\lambda} + 2 \frac{\cos(\theta)}{\sin(\theta)} \frac{d\theta}{d\lambda} \frac{d\phi}{d\lambda} = 0 \end{aligned}$$

Notice that the differential equation for the first variable  $t$ , completely disappears. This is due to the fact that all the Christoffel symbols for time are zero so this equation vanishes. We want to rewrite the resulting system of second order differential equations

to system of first order differential equations. In order to do so we introduce three new variables this time:  $v^1, v^2$  and  $v^3$  which will represent the first-order derivatives. Notice how we skip upper index 0 since the  $t$  velocity vanishes. This gives us the following first-order system of ordinary differential equations.

$$\begin{aligned}\frac{dv^1}{d\lambda} &= r(v^2)^2 + r \sin(\theta)^2(v^3)^2 \\ \frac{dv^2}{d\lambda} &= -2\frac{v^2v^1}{r} + \sin(\theta) \cos(\theta)(v^3)^2 \\ \frac{dv^3}{d\lambda} &= -2\frac{v^3v^1}{r} - 2\frac{\cos(\theta)}{\sin(\theta)}v^2v^3 \\ \frac{dr}{d\lambda} &= v^1 \\ \frac{d\theta}{d\lambda} &= v^2 \\ \frac{d\phi}{d\lambda} &= v^3\end{aligned}$$

## 6.5 Solving the system of differential equations

We want to solve the defined system of differential equations to determine the geodesics in Minkowski space and visualise them. Since Minkowski space is basically three-dimensional Euclidean space with an extra dimension of time, we expect geodesics to be straight lines. This makes sense since the force of gravity is not present so there's no curvature of spacetime. I use the same Python solver as in subsection (5.6) but with adjusted differential equations and adjusted initial conditions of course. Next to the solver I also implemented the Euler-method by hand to have some sort of check on the results of the Python solver. I set all variables that require an initial value (six in total) equal to 1 to get an impression of what the geodesics will look like. The repeated value of 1 is basically randomly determined, however it made sense to keep on using 1 like we did in the previous section. When our solver and Euler-method are up and running we can start plotting to visualise the geodesics. We start by plotting the trajectories of  $r, \theta$  and  $\phi$  of the specific geodesic in Minkowski space given our initial conditions.

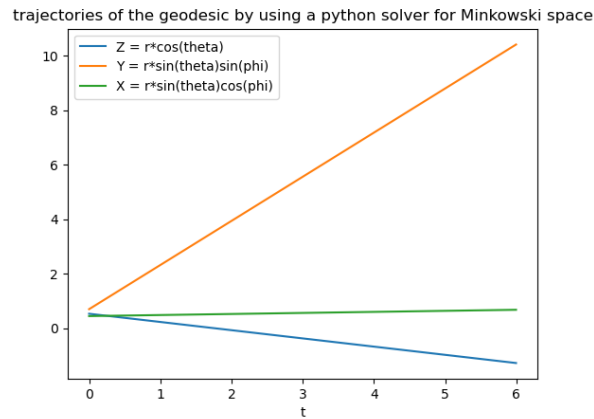


Figure 6: The trajectories of the variables  $r$ ,  $\theta$  and  $\phi$  of the geodesic expressed in spherical coordinates (with initial conditions set to  $(1,1,1,1,1,1)$ ) for Minkowski space.

We can clearly see that the trajectory of the geodesic in  $X$ ,  $Y$  and  $Z$  direction all consists out of straight lines. Notice that our initial condition was basically arbitrary chosen and resulted into straight trajectories. This shows that most likely all geodesics given various initial conditions will turn out to be straight lines. In order to confirm this, I plotted the trajectories given different initial conditions. Though the trajectories can differ very much in between each other they were all straight trajectories, as can be seen in the figures below.

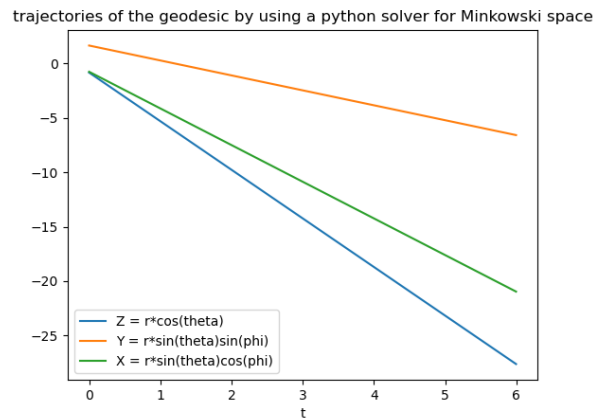


Figure 7: The trajectories of the variables  $r$ ,  $\theta$  and  $\phi$  of the geodesic expressed in spherical coordinates (with initial conditions set to  $(2,2,2,2,2,2)$ ) for Minkowski space.

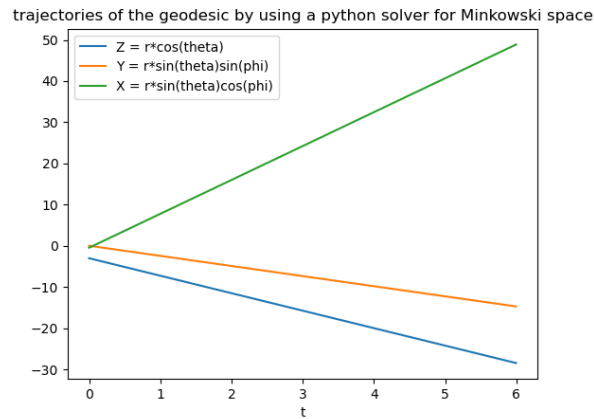


Figure 8: The trajectories of the variables  $r$ ,  $\theta$  and  $\phi$  of the geodesic expressed in spherical coordinates (with initial conditions set to  $(3,3,3,3,3,3)$ ) for Minkowski space.

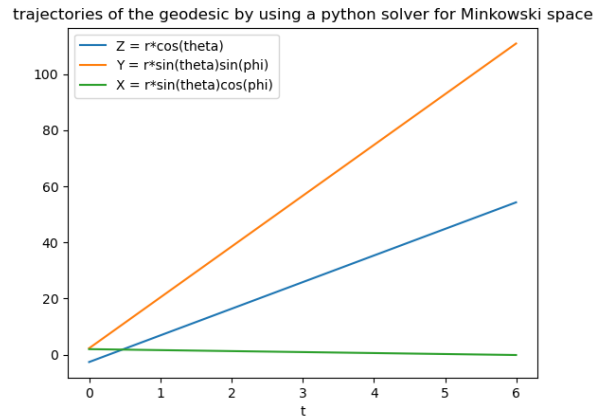


Figure 9: The trajectories of the variables  $r$ ,  $\theta$  and  $\phi$  of the geodesic expressed in spherical coordinates (with initial conditions set to  $(4,4,4,4,4,4)$ ) for Minkowski space.

Now that we know we are dealing with straight lines and have an idea of what the trajectories look like, we can plot the Minkowski geodesics in three-dimensional space. We would actually like to plot in four-dimensional space since Minkowski space is four-dimensional, but doing so in an image is physically impossible. Besides we know that the time variable  $t$  is not apparent in the system of differential equations, so this can be left out. Therefore a three-dimensional space is sufficient for the visual plot of all variables involved.

3D plot of the geodesic by using a python solver for Minkowski space

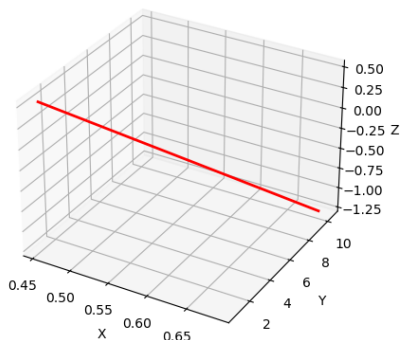


Figure 10: The three-dimensional plot of the Minkowski geodesic given the initial conditions  $(1,1,1,1,1)$ .

And yet again we see that we are dealing with a straight line.

It may seem a bit unnecessary to go through all this trouble if we already knew we would plot straight lines, which is not that interesting at all. Implementing the system of differential equations as well as the plotters actually really helps us in setting up the required tools for the Schwarzschild metric. That is why it was so important.

## 6.6 Setting the initial condition of light rays

In this section we make a start with the implementation of the image transformation i.e. simulate the light ray trajectories. More specifically this section focuses on the initial requirements needed to properly simulate the trajectories of the light rays in our metric. With initial conditions we mean a starting point and a velocity in each spatial direction for each individual light ray. In this section we'll be mathematically deriving how to properly set these initial conditions to meet our requirements.

We'll start by covering the requirements we want to set for our light rays.

- All light rays start from the same plane.
- The light ray field is constructed in such a way that  $X = Y = 0$  is located in the center.
- All light rays have the same initial velocity.
- All light rays travel perpendicular to the plane they start from in positive direction.

The first requirement is set so that all light rays start aligned. We have chosen to position all light rays at  $Z = -10$ , spread out in the  $x, y$ -plane.

The second requirement is set because in the Schwarzschild metric the black hole will be located in the origin so we want our light rays to surround the  $X = Y = 0$  center symmetrically.

To place the starting positions of the light rays in the  $x, y$ -plane at  $Z = -10$  means we are defining these particular starting point in terms of the  $x, y, z$ -plane by its Cartesian coordinate. However our  $X, Y, Z$  values are expressed by the spherical coordinate system. This means we need to be able to switch from the Cartesian to the spherical coordinate system. In order to perform this transformations we use the following formulas, given a specified  $X, Y, Z$ -coordinate.

$$\begin{aligned} r &= \sqrt{X^2 + Y^2 + Z^2} \\ \theta &= \arccos\left(\frac{Z}{r}\right) \\ \phi &= \arctan 2(YX) \end{aligned}$$

Where we define  $\arctan 2$  in such a way that,

$$\arctan 2(y, x) = \begin{cases} \arctan\left(\frac{y}{x}\right) & \text{if } x > 0, \\ \arctan\left(\frac{y}{x}\right) + \pi & \text{if } x < 0 \text{ and } y \geq 0, \\ \arctan\left(\frac{y}{x}\right) - \pi & \text{if } x < 0 \text{ and } y < 0, \\ +\frac{\pi}{2} & \text{if } x = 0 \text{ and } y > 0, \\ -\frac{\pi}{2} & \text{if } x = 0 \text{ and } y < 0, \\ \text{undefined} & \text{if } x = 0 \text{ and } y = 0. \end{cases}$$

Note that the initial condition exists out of an initial coordinate and initial velocities. Therefore we still have to define these initial velocities which are specified by the third and fourth requirement. Our third requirement is set so that way all light rays travel the same distance within a specified time frame. We choose to set all velocities equal to 1.

Finally the last requirement is set so that all light rays travel straight towards the  $z = 0$ -plane. Perpendicular to the  $z$ -plane means there won't be any velocity in the  $z$ -direction so the  $z$  velocity is set to 0.

The velocities are described by means of spherical coordinates as well, so not Cartesian. Again we have to transition from Cartesian to spherical. This time It is a little bit

more tricky so we use the multi-variable chain rule as we did in section (5).

$$\begin{aligned}
v^1 &= \frac{dr}{d\lambda} = \frac{\partial r}{\partial X} \frac{dX}{d\lambda} + \frac{\partial r}{\partial Y} \frac{dY}{d\lambda} = \frac{\partial r}{\partial Z} \frac{dZ}{d\lambda} \\
&= \frac{X}{\sqrt{X^2 + Y^2 + Z^2}} v_X + \frac{Y}{\sqrt{X^2 + Y^2 + Z^2}} v_Y + \frac{Z}{\sqrt{X^2 + Y^2 + Z^2}} v_Z \\
v^2 &= \frac{d\theta}{d\lambda} = \frac{d\theta}{\partial X} \frac{dX}{d\lambda} + \frac{\partial \theta}{\partial Y} \frac{dY}{d\lambda} = \frac{d\theta}{\partial Z} \frac{dZ}{d\lambda} \\
&= \frac{XZ}{\sqrt{X^2 + Y^2}(X^2 + Y^2 + Z^2)} v_X + \frac{YZ}{\sqrt{X^2 + Y^2}(X^2 + Y^2 + Z^2)} v_Y + \\
&\quad \frac{-X^2 - Y^2}{\sqrt{X^2 + Y^2}(X^2 + Y^2 + Z^2)} v_Z \\
v^3 &= \frac{d\phi}{d\lambda} = \frac{\partial \phi}{\partial X} \frac{dX}{d\lambda} + \frac{\partial \phi}{\partial Y} \frac{dY}{d\lambda} + \frac{\partial \phi}{\partial Z} \frac{dZ}{d\lambda} = -\frac{Y}{X^2 + Y^2} v_X + \frac{X}{X^2 + Y^2} v_Y
\end{aligned}$$

For each light ray we can specify its initial position in Cartesian coordinates:  $(X, Y, -10)$  as well as its initial Cartesian velocities  $(1, 1, 0)$ . Both will be transformed to the spherical plane which is used throughout this thesis. This means we have constructed the initial condition for each light ray that matches our requirements which is a big step towards completely simulating the light rays.

## 6.7 Plotting light rays

In this section we'll actually be plotting light rays in a three dimensional space. A disclaimer however, this all won't be too excited since Minkowski space is not curved. Nonetheless implementing this three-dimensional visualisation will lay the foundation for visualizing light rays in the Schwarzschild metric.

In the previous subsection (6.6) we determined how to set up the initial conditions for the light rays. However a number of aspects are still missing in order to properly visualise the light rays. First of all we need to define a field size. This determines the size of the  $X$  and  $Y$  interval at  $Z = -10$  from where the light rays will start. Note that as previously mentioned, the  $X, Y$  interval is transposed in such a way that  $X = Y = 0$  in the center. We'll start off with a really small field size: 6x6. This assures that the light rays will be clearly visible instead of seeing one big chunk of indistinguishable rays. Second of all we need to determine which  $X, Y$  values in the  $Z = -10$  plane we pick to start of. Again we want to avoid creating a concentrated mass of light rays so we require them to have proper distance between each other. We find that if we take only integer values within the  $X \times Y$  interval the geodesics will meet this requirement. For each light ray starting in the  $X \times Y$  interval with integer values, the trajectory is computed through the geodesic constructor function. This function takes the  $X$  and  $Y$  starting coordinates, the time step and end time as inputs. The time step still remains 0.005 and the end time is set to 20. This end time is chosen in such a way that the geodesics end is located at  $Z = 10$ , in this way the light rays travel as much below the origin as above it with

respect to the  $z$ -axis.

The initial Cartesian condition is constructed:  $(X_{\text{start}}, Y_{\text{start}}, -10, 0, 0, 1)$  and is converted to spherical by the formulas of the previous subsection (6.6). This converted initial condition is fed into the Python Minkowski solver which will construct a list of  $r, \theta$  and  $\phi$  values throughout the time interval. These lists are converted back to Cartesian  $X, Y, Z$  - coordinate lists so we know the relative end coordinates. The complete trajectories of the light rays are plotted according to these three lists by means of a plotter.

There remains one issue, the geodesic through the origin is not defined. That is due to the fact that the origin is not defined in spherical coordinates. We solve this issue by simply leaving this specific geodesic out completely. We are now fully equipped to plot the geodesics in Minkowski space.

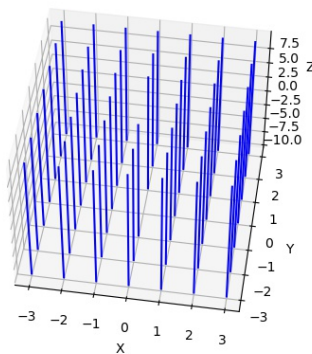


Figure 11: The three-dimensional plot of the Minkowski geodesics given field size of 6, a  $dt$  of 0.005 and a  $t_{\text{end}}$  of 20.

Notice that indeed there's no geodesic in the origin. Furthermore all geodesics are perpendicular to the  $Z = -10$ -plane, all geodesics start in the same plane  $Z = -10$ , all geodesics have equal positive velocity, the field size is 6 and all geodesics start at integer  $X, Y$ -values i.e. all our requirements are met. As briefly mentioned before the fact that Minkowski space is not curved means the light rays will just be straight lines. Not too exciting but the entire simulating procedure can be carried over to the Schwarzschild metric.

We mentioned that  $(X_{\text{start}}, Y_{\text{start}})$  and the total trajectories of the geodesics in terms of the Cartesian coordinates of each geodesic is determined. Notice that if we take the last element of the list of  $X$  and  $Y$  values of the geodesic trajectory we have  $(X_{\text{end}}, Y_{\text{end}})$ . We are interested in these coordinates since this allows us to construct a before and after

image by means of a scatter plot. This gives a clear visualisation of where the geodesics start and where they will end without plotting the entire trajectory.

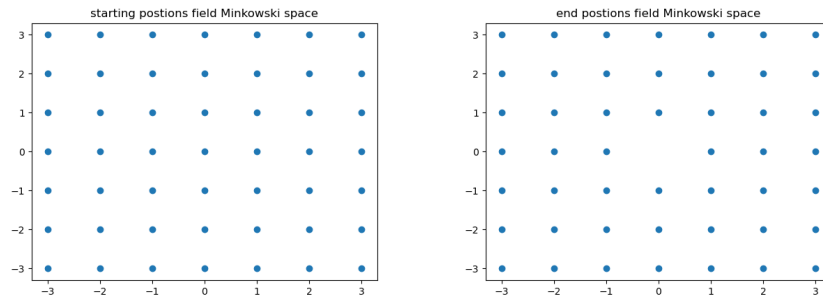


Figure 12: Left: the starting positions of all the geodesics in the 6x6 field, right: the end positions of all the geodesics in the 6x6 field (the origin is missing).

Again not very special since we are dealing with a set of parallel straight lines. We see that every geodesics starting point is mapped to itself except for the origin, since the origin is not defined in spherical coordinates. Once we are dealing with the Schwarzschild metric this form of mapping visualisation will prove to be very interesting.

## 6.8 Transforming images

In the previous subsection (6.7) we were able to determine the trajectories of our specified geodesics (containing initial conditions which met all the requirements) and visualise them. We are going to use this knowledge to derive the way an image will be transformed in Minkowski space, where the image is projected from  $Z = -10$  to the observer at  $Z = 10$ . We will start by explaining our approach for this projection. The approach which we'll be using for this visualisation will be the exact same for the Schwarzschild metric so the work we are doing here is very useful.

We start by placing an input image in the  $x, y$ -plane at  $Z = -10$ . Each pixel of the input image, identified by its row index and column index is mapped to an  $X, Y$  value. In order to continue it is important to know how pixels 'work'. In Python a pixel is represented by an RGB (red, green, blue) value list. Basically any color can be created by a combination of a specific shade of red, green and blue. This shade of each color is represented by a value anywhere between 0 and 255, where 0 corresponds to black and 255 to white. The RGB value list for each pixel therefore consists out of three integers all varying between 0 and 255.

Second of all it is important to note how we loop over the pixels of our image. We start at `pixel[0,0]` which corresponds to the pixel on the top left corner, we then continue to the pixel to the right i.e. `pixel[0,1]` up until we reach the last pixel of that row in the top right corner. We then move over to the second row, `pixel[1,0]`, until eventually we

reach the last pixel i.e. pixel[number of width pixels, number of height pixels].

Remember that the entire plane occupied by the input image will be transposed in the  $X, Y$ -plane such that  $X = Y = 0$  lies in the center of the image. Therefore these pixel row and column index need to be transposed as well. In order to conform to this transposition, we map (pixel column index, pixel row index) to ( $X_{\text{start}} = - \text{number of width pixels} / 2 + \text{pixel column index}$ ,  $Y_{\text{start}} = \text{number of height pixels} / 2 - \text{pixel row index}$ ).

For each individual pixel, a geodesic will be computed which in Minkowski space means a system of 6 coupled differential equations needs to be solved given the prescribed initial conditions (with  $X = X_{\text{start}}, Y = Y_{\text{start}}$ ). Once the geodesic is computed, the  $X_{\text{end}}$  and  $Y_{\text{end}}$  coordinate can be determined by converting the  $r, \theta$  and  $\phi$  solution lists to  $X, Y$ , solution lists and taking the last value of both. Now this  $X_{\text{end}}$  and  $Y_{\text{end}}$  values need to be converted back to a pixel index and pixel row. This is done by taking the inverse of the original transformation: pixel column index =  $X_{\text{end}} + \text{number of width pixels} / 2$ , pixel row index =  $Y_{\text{end}} - \text{number of height pixels} / 2$  and rounding these to integer values. Now we know exactly where each pixel from the input image is being mapped to.

We then create an output image with the exact same size as the input image and set every pixel to black to start off. For each pixel in the input image (starting from top left) the RGB value list of this 'start' pixel is determined. We calculate to what 'end' pixel this 'start' pixel is being mapped to by solving the geodesic equation by means of the just described method. The RGB value list of the 'start' pixel position of the output image is set to RGB value of the 'end pixel' position of the input image. Notice that in this way every pixel in the output image will have an RGB value originated from the input image, which means we have a surjective mapping. Furthermore no pixel values will be stacked, i.e. every pixel's RGB value list in the output image has a unique origin pixel RGB list value from the input image. The approach can perhaps best be described by the following image.

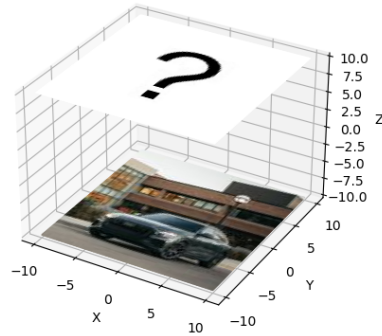


Figure 13: The input image is displayed at  $Z = -10$  in the  $X, Y$ - field, such that the center of the image is at  $X = Y = 0$ . The image is projected through the plane  $Z = 0$  until it reaches the plane where  $Z = 10$ . The output/projected image is yet unknown and therefore carries the question mark.

I implemented this described method in Python. If you run the program, the output image gets constructed real time meaning that you can see that every black pixel is changed to the corresponding correct pixel RGB value list. Unfortunately I cannot show this feature in the thesis, but the code can be ran by yourself of course. Remember that we are dealing with the Minkowski space, i.e. the geodesics are straight lines. This means that for every pixel at position  $(X, Y)$  we have that  $X_{\text{start}} = X_{\text{end}}$  and  $Y_{\text{start}} = Y_{\text{end}}$ , except for the origin. The origin pixel in the output image will remain black since this geodesic is left out. This means the output image is identical to the input image except for 1 black pixel in the center. This notion becomes very visible if we compare the input image with the output image in the following figure. We use a 100x100 pixel image so the computation time will be manageable (unfortunately the resolution will be lower).



Figure 14: Left: the 100x100 input image in Minkowski space, right: the 100x100 output image in Minkowski space.

We see that indeed the images are the same except for the center pixel of the output image. I managed to improve the program in such a way that it ran a lot faster. This means I could compute the output image for input images with a lot higher resolution as well. However, the input and output image will still remain the same except for the center pixel which will become less visible by increasing the resolution. Therefore It is not really interesting to show these images.

We return to figure 13 and are now able to replace the question mark by the actual transformed image.

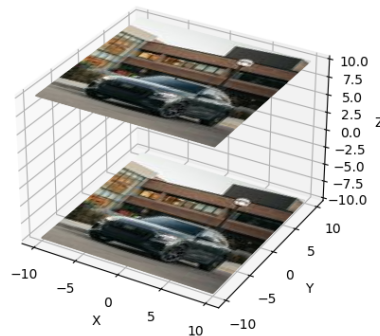


Figure 15: The input image is displayed at  $Z = -10$  in the  $X, Y$ - field, such that the center of the image is at  $X = Y = 0$ . The image is projected through the plane  $Z = 0$  until it reaches the plane where  $Z = 10$ . The output/projected image displayed at  $Z = 10$ .

We made some major steps with respect to setting the initial conditions, finding the geodesics and transforming the image. This allows us to finally take the big step to start working on the Schwarzschild metric.

## 7 Schwarzschild metric

In this section we will be simulating the presence of a black hole and see how this alters things with respect to all our previous results. In the end we will be able to construct the image from the perspective of the observer in front of the black hole which was exactly our original goal.

### 7.1 Defining the metric

The Schwarzschild metric in spherical coordinates is given as:

$$ds^2 = \left(1 - \frac{r_s}{r}\right) dt^2 - \frac{dr^2}{1 - \frac{r_s}{r}} - r^2 d\theta^2 - r^2 \sin(\theta) d\phi^2 \quad (27)$$

Before we start It is perhaps a good idea to clarify some aspects of the metric. First of all notice that all the the variables are familiar to us from the Minkowski metric. Besides the variables, the appearance of  $r_s$  is very prominent in the metric. This  $r_s$  represents the Schwarzschild radius of the black hole. Notice that Minkowski space is completely recovered when  $\frac{r_s}{r}$  goes to zero. We will show that this is the case by taking  $r_s = 0$  and visualising the curvature of the light rays (they should be straight lines).

### 7.2 Determining the metric tensor

The corresponding metric tensor is given by,

$$g_{ij} = \begin{pmatrix} 1 - \frac{r_s}{r} & 0 & 0 & 0 \\ 0 & -\frac{1}{1 - \frac{r_s}{r}} & 0 & 0 \\ 0 & 0 & -r^2 & 0 \\ 0 & 0 & 0 & -r^2 \sin(\theta)^2 \end{pmatrix} \quad (28)$$

while the inverse metric tensor is given by,

$$g^{ij} = \begin{pmatrix} \frac{1}{1 - \frac{r_s}{r}} & 0 & 0 & 0 \\ 0 & -1 + \frac{r_s}{r} & 0 & 0 \\ 0 & 0 & -\frac{1}{r^2} & 0 \\ 0 & 0 & 0 & -\frac{1}{r^2 \sin(\theta)^2} \end{pmatrix} \quad (29)$$

### 7.3 Determining the Christoffel symbols

We use formula (17) to determine all Christoffel symbols. Since we have some experience with calculating the Christoffel symbols from the Minkowski space, we are going to omit the excessive steps. We use the notation described by (18). We start by substituting our first entry  $t$  where we use the fact that  $g^{0\alpha} = 0$  for all  $\alpha \neq 0$ , so we can substitute  $\alpha = 0$ :  $g^{00}$  right away.

$$\Gamma_{ij}^0 = \frac{1}{2} g^{00} (g_{0i,j} + g_{0j,i} - g_{ij,0})$$

Not a singly entry in the metric tensor metric is dependent of  $t$  so  $g_{ij,0} = 0$  for all  $i, j$  so all partial derivatives to  $t$  vanish, which gives,

$$\Gamma_{ij}^0 = \frac{1}{2}g^{00}(g_{0i,j} + g_{0j,i})$$

Now  $g_{0k}$  is only non-zero when  $k = 0$ , however  $g_{00,0} = 0$  so we must have  $j \neq 0$  and  $i = 0$ ,  $g_{00,j}$  is then only non-zero when  $j = 1$  so we have,

$$\Gamma_{01}^0 = \frac{1}{2} \frac{1}{(1 - \frac{r_s}{r})} \frac{\partial}{\partial r} \left(1 - \frac{r_s}{r}\right) = \frac{1}{2} \frac{-1}{(1 - \frac{r_s}{r})} \frac{r_s}{r^2} = \frac{-r_s}{2r(r - r_s)}$$

By (16) we have,

$$\Gamma_{10}^0 = \Gamma_{01}^0 = \frac{-r_s}{2r(r - r_s)}$$

We now substitute our next entry  $r$  into (17) where we use again the fact that the inverse metric tensor is only non-zero for  $\alpha = 1$ . We have that,

$$\Gamma_{ij}^1 = \frac{1}{2}g^{11}(g_{1i,j} + g_{1j,i} - g_{ij,1})$$

If we take  $i = 0, j = 0$  we have,

$$\Gamma_{00}^1 = \frac{1}{2}g^{11}(g_{10,0} + g_{10,0} - g_{00,1}) = -\frac{1}{2}g^{11}g_{00,1} = \frac{1}{2} \cdot - \left(-1 + \frac{r_s}{r}\right) \cdot \frac{r_s}{r^2} = \frac{r_s(r - r_s)}{2r^3}$$

If we take  $i = 1, j = 1$  we have,

$$\Gamma_{11}^1 = \frac{1}{2}g^{11}(g_{11,1} + g_{11,1} - g_{11,1}) = \frac{1}{2}g^{11}g_{11,1} = \frac{1}{2} \cdot \left(-1 + \frac{r_s}{r}\right) \cdot \frac{r_s}{(r - r_s)^2} = -\frac{r_s}{2r(r - r_s)}$$

If we take  $i = 2, j = 2$  we have,

$$\Gamma_{22}^1 = \frac{1}{2}g^{11}(g_{12,2} + g_{12,2} - g_{22,1}) = -\frac{1}{2}g^{11}g_{22,1} = -\frac{1}{2} \cdot \left(-1 + \frac{r_s}{r}\right) \cdot -2r = -(r - r_s)$$

If we take  $i = 3, j = 3$  we have,

$$\Gamma_{33}^1 = \frac{1}{2}g^{11}(g_{13,3} + g_{13,3} - g_{33,1}) = -\frac{1}{2}g^{11}g_{33,1} = -\frac{1}{2} \cdot \left(-1 + \frac{r_s}{r}\right) \cdot -2r \sin(\theta)^2 = -(r - r_s) \sin(\theta)^2$$

Now we move on to the third variable  $\theta$  which we substitute into (17). Again we have that only for  $\alpha \neq 0$  we have that  $\alpha = 2$  so we get,

$$\Gamma_{ij}^2 = \frac{1}{2}g^{22}(g_{2i,j} + g_{2j,i} - g_{ij,2})$$

A non-zero Christoffel symbol given upper index  $\theta$  is achieved when we take  $i = 1$  and  $j = 2$  since we have,

$$\Gamma_{12}^2 = \frac{1}{2}g^{22}(g_{21,2} + g_{22,1} - g_{12,2}) = \frac{1}{2} \cdot -\frac{1}{r^2} \cdot -2r = \frac{1}{r}$$

And by symmetry of the lower index of Christoffel symbols we have that ,

$$\Gamma_{12}^2 = \Gamma_{21}^2 = \frac{1}{r}$$

By taking  $i = 3$  and  $j = 3$  we have that,

$$\Gamma_{33}^2 = \frac{1}{2}g^{22}(g_{23,3} + g_{23,3} - g_{33,2}) = \frac{1}{2} \cdot -\frac{1}{r^2} \cdot 2r^2 \sin(\theta) \cos(\theta) = -\sin(\theta) \cos(\theta)$$

All other Christoffel symbols for upper index 3 are zero. Now we move on to the fourth and final variable  $\phi$  which carries index 3. We substitute this value into the formula (17). Again we have that only for  $\alpha \neq 0$  we have that  $\alpha = 3$  so we get,

$$\Gamma_{ij}^3 = \frac{1}{2}g^{33}(g_{3i,j} + g_{3j,i} - g_{ij,3}) = -\frac{g_{3i,j} + g_{3j,i} - g_{ij,3}}{2r^2 \sin(\theta)}$$

By taking  $i = 1$  and  $j = 3$  we have that,

$$\Gamma_{13}^3 = \frac{1}{2}g^{33}(g_{31,3} + g_{33,1} - g_{13,3}) = -\frac{-2r \sin(\theta)^2}{2r^2 \sin(\theta)} = \frac{1}{r}$$

By the symmetry of lower indices of Christoffel symbols we have by (16),

$$\Gamma_{13}^3 = \Gamma_{31}^3 = \frac{1}{r}$$

Finally if we take  $i = 2, j = 3$  we have that,

$$\Gamma_{23}^3 = \frac{1}{2}g^{33}(g_{32,3} + g_{33,2} - g_{23,3}) = -\frac{-2r^2 \sin(\theta) \cos(\theta)}{2r^2 \sin(\theta)} = \frac{\cos(\theta)}{\sin(\theta)}$$

By the symmetry of lower indices of Christoffel symbols we have by (16),

$$\Gamma_{32}^3 = \Gamma_{32}^3 = \frac{\cos(\theta)}{\sin(\theta)}$$

## 7.4 Deriving the system of differential equations

We clearly have a lot more non-zero Christoffel symbols than we did in Minkowski space. This means that we have more expressions in the coupled differential equations. Most notably there are Christoffel symbols with upper index 0 which are non-zero, meaning we have an extra equation in the system. We determine the system of differential equations analogous to the Minkowski and Euclidean metric.

$$\begin{aligned}
\frac{d^2 u^0}{d\lambda^2} + (\Gamma_{01}^0 + \Gamma_{10}^0) \frac{du^0}{d\lambda} \frac{du^1}{d\lambda} &= \frac{d^2 t}{d\lambda^2} - \frac{r_s}{r(r-r_s)} \frac{dt}{d\lambda} \frac{dr}{d\lambda} = 0 \\
\frac{d^2 u^1}{d\lambda^2} + \Gamma_{00}^1 \left( \frac{du^0}{d\lambda} \right)^2 + \Gamma_{11}^1 \left( \frac{du^1}{d\lambda} \right)^2 + \Gamma_{22}^1 \left( \frac{du^2}{d\lambda} \right)^2 + \Gamma_{33}^1 \left( \frac{du^3}{d\lambda} \right)^2 &= \\
\frac{d^2 r}{d\lambda^2} + \frac{r_s(r-r_s)}{2r^3} \left( \frac{dt}{d\lambda} \right)^2 - \frac{r_s}{2r(r-r_s)} \left( \frac{dr}{d\lambda} \right)^2 - (r-r_s) \left( \left( \frac{d\theta}{d\lambda} \right)^2 + \sin^2(\theta) \left( \frac{d\phi}{d\lambda} \right)^2 \right) &= 0 \\
\frac{d^2 u^2}{d\lambda^2} + (\Gamma_{12}^2 + \Gamma_{21}^2) \frac{du^2}{d\lambda} \frac{du^1}{d\lambda} + \Gamma_{33}^2 \left( \frac{du^3}{d\lambda} \right)^2 &= \frac{d^2 \theta}{d\lambda^2} + \frac{2}{r} \frac{d\theta}{d\lambda} \frac{dr}{d\lambda} - \sin(\theta) \cos(\theta) \left( \frac{d\phi}{d\lambda} \right)^2 = 0 \\
\frac{d^2 u^3}{d\lambda^2} + (\Gamma_{13}^3 + \Gamma_{31}^3) \frac{du^1}{d\lambda} \frac{du^3}{d\lambda} + (\Gamma_{23}^3 + \Gamma_{32}^3) \frac{du^2}{d\lambda} \frac{du^3}{d\lambda} &= \frac{d^2 \phi}{d\lambda^2} + \frac{2}{r} \frac{dr}{d\lambda} \frac{d\phi}{d\lambda} + 2 \frac{\cos(\theta)}{\sin(\theta)} \frac{d\theta}{d\lambda} \frac{d\phi}{d\lambda} = 0
\end{aligned}$$

We rewrite this system of 4 second order differential equations to a system of 8 first order differential equations as we have done before.

$$\begin{aligned}
\frac{dv^0}{d\lambda} &= \frac{r_s}{r(r-r_s)} v^0 v^1 \\
\frac{dv^1}{d\lambda} &= -\frac{r_s(r-r_s)}{2r^3} (v^0)^2 + \frac{r_s}{2r(r-r_s)} (v^1)^2 + (r-r_s) ((v^2)^2 + \sin^2(\theta) (v^3)^2) \\
\frac{dv^2}{d\lambda} &= -\frac{2}{r} v^2 v^1 + \sin(\theta) \cos(\theta) (v^3)^2 \\
\frac{dv^3}{d\lambda} &= -\frac{2}{r} v^1 v^3 - 2 \frac{\cos(\theta)}{\sin(\theta)} v^2 v^3 \\
v^0 &= \frac{dt}{d\lambda} \\
v^1 &= \frac{dr}{d\lambda} \\
v^2 &= \frac{d\theta}{d\lambda} \\
v^3 &= \frac{d\phi}{d\lambda}
\end{aligned}$$

## 7.5 Solving the system of differential equations

I implemented solvers for the system of differential equations by using Euler's-method as well as by the pre-built solver we are familiar with. We can start off by defining some random initial condition and see what the geodesic will look like. To continue in a similar fashion we take (1,1,1,1,1,1,1,1) as the initial condition. Notice that the initial condition has moved up from 6 values in Minkowski space to 8 values in the Schwarzschild metric. Besides the initial condition we also have to specify the value of  $r_s$  (the Schwarzschild radius). A large value of  $r_s$  corresponds to a large field of curvature and a small value to a small field of curvature. In fact setting  $r_s$  to 0 should result in the Minkowski space. We'll show that this holds given our initial condition first.

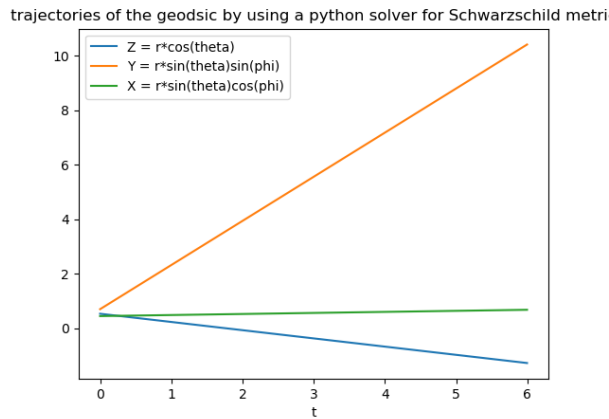


Figure 16: The trajectories of the variables  $r, \theta$  and  $\phi$  of the geodesic expressed in spherical coordinate (with initial condition set to  $(1,1,1,1,1,1,1)$ ) for the Schwarzschild metric with  $r_s$  set to 0.

If we compare this image to the Minkowski trajectory visualised in image 9, we see that we are dealing with the exact same trajectories. Indeed  $r_s = 0$  gives us the Minkowski space in this case.

Changing our value of  $r_s$  however significantly alters the trajectories. If we pick  $r_s$  to be 0.8 for instance the output is the following.

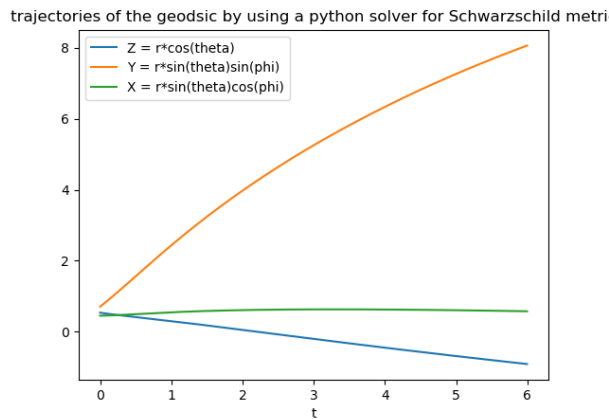


Figure 17: The trajectories of the variables  $r, \theta$  and  $\phi$  of the geodesic expressed in spherical coordinate (with initial condition set to  $(1,1,1,1,1,1,1)$ ) for the Schwarzschild metric with  $r_s$  set to 0.8.

Clearly these trajectories differ from the Minkowski trajectories so the  $r_s$  value most definitely influences the geodesic trajectory.

## 7.6 Defining the $t$ velocity

Everything we covered in subsection (6.6) can be carried over to the Schwarzschild metric, which saves us a lot of work. We have one remaining issue however. In the Minkowski space the first equation, involving the  $t$  variable vanished since all the Christoffel symbols with upper index 0 were zero. In the Schwarzschild metric, this is not the case anymore. This means we have an extra equation in the system of differential equations and therefore require an extra initial value: the  $t$  velocity. This velocity can be determined by what's known as a *null-geodesic*. Massless particles like photons follow these null-geodesics which are described by.

$$g_{ij} \frac{dx^i}{ds} \frac{dx^j}{ds} = 0 \quad (30)$$

We have that  $g_{ij} \neq 0$  only if  $i = j$  which gives,

$$\begin{aligned} (v^0)^2 &= \frac{-\frac{dx^1}{ds} \frac{dx^1}{ds} g_{11} - \frac{dx^2}{ds} \frac{dx^2}{ds} 2g_{22} - \frac{dx^3}{ds} \frac{dx^3}{ds} g_{33}}{g_{00}} = \frac{-(v^1)^2 g_{11} - (v^2)^2 g_{22} - (v^3)^2 g_{33}}{g_{00}} \\ &= \frac{-(v^1)^2 \left(-\frac{1}{1-\frac{r_s}{r}}\right) - (v^2)^2 (-r^2) - (v^3)^2 (-r^2 \sin(\theta))}{\left(1 - \frac{r_s}{r}\right)} \end{aligned}$$

So we have that,

$$v^0 = \sqrt{\frac{(v^1)^2 \left(\frac{1}{1-\frac{r_s}{r}}\right) + (v^2)^2 r^2 + (v^3)^2 r^2 \sin(\theta)}{\left(1 - \frac{r_s}{r}\right)}}$$

This formula is programmed in Python which enables us to determine the  $v^0$  initial velocity given the other initial velocities. Remember that these other initial velocities ( $v^1, v^2, v^3$ ) are all calculated by means of the spherical transformation formulas which transforms the Cartesian initial velocities  $v^x, v^y, v^z = (1, 1, 0)$  to their relative spherical expression as described in subsection (6.6). Since all the light rays have equal initial velocities all the initial velocities:  $v^0, v^1, v^2, v^3$  are the same for each geodesic and can be predetermined.

## 7.7 Plotting light rays

In this subsection we'll actually be plotting light rays in a three dimensional space just like we did for the Minkowski space. In fact everything covered in section (6.7) can be carried over to the Schwarzschild metric. The only difference is that we have a more advanced system of differential equations and an expanded initial condition. Unlike the previous section, the light rays of the Schwarzschild metric will prove to be very interesting. We'll show this by plotting the light rays given various values of  $t$ . Throughout this subsection we use a the same 6x6 field and take  $r_s = 1$  which means we are dealing with some serious curvature.

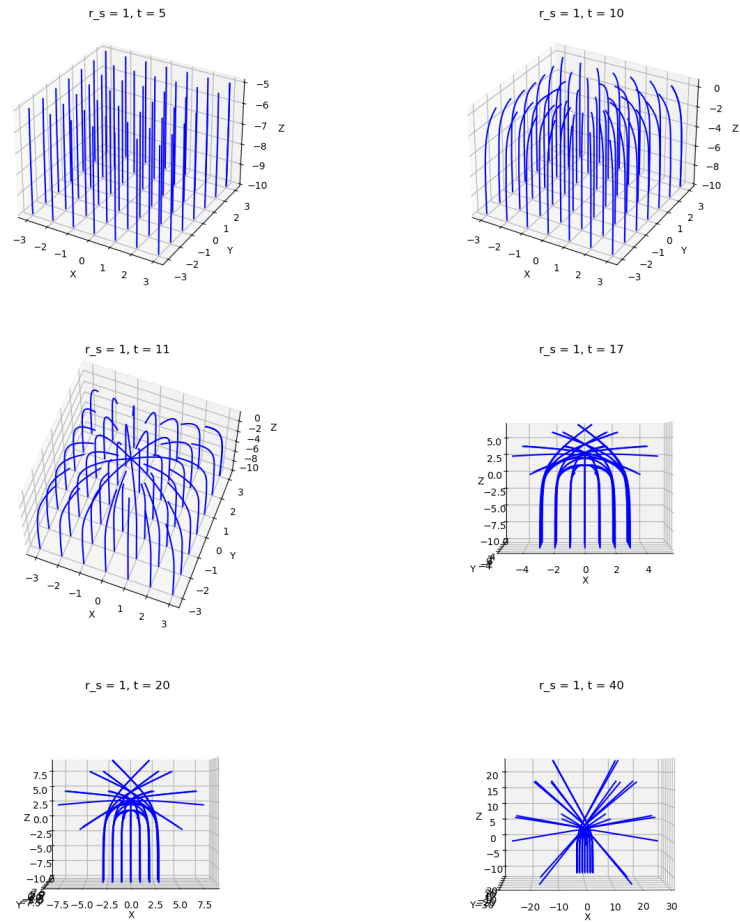


Figure 18: Several plots visualizing the trajectory of light rays at different  $t$  values in the Schwarzschild metric with  $r_s = 1$ .

We are going to walk through each plot starting from top left, to observe how the geodesics progress over time.

For our first plot we picked  $t = 5$ . We see that all geodesics start off as straight lines which look familiar to us from the Minkowski space. Notice that the geodesic in the origin is missing since the spherical coordinate system is not defined there. The geodesics are still quite far from the black hole in the origin, meaning that the light rays are barely effected by its gravitational pull. Therefore it makes sense that we are dealing with straight lines.

When we double  $t$  to 10 we start to notice the occurrence of some curvature already. The light rays barely passed the  $X = Y = 0$  -plane, meaning the origin geodesic (if it was still there) would be located within the Schwarzschild radius.

Only 1 time step further, at  $t = 11$  we see that there is a lot more curvature and light rays are actually intersecting above the black hole.

When we move on to  $t = 17$  the image gets very messy because of all the different trajectories so I changed the point of view to one where we do not see any depth in the  $y$ -direction. Here we notice that the end positions of the light rays are located in completely different  $Z$  positions. Unlike the Minkowski space, the light rays aren't aligned at all. Some geodesics undergo such extreme curvature that they are actually pulled back towards  $Z = -10$  where they started.

At  $t = 20$  we see that some light rays even interchanged position compared to their starting point. This means this section will be upside down for the observer!

Lastly at  $t = 40$  It is evident that there is a huge difference between the light ray's  $X, Y$ -end positions and  $X, Y$  starting position.

Remember that our aim is to construct the image from the point of view of the observer located at the plane  $Z = 10$ . In our new metric this means we have to apply some conditions to our geodesics.

First of all, we leave out all the geodesics that never reach  $Z = 10$ , since they will never reach the observer. We remove these geodesics by setting  $t_{\text{end}}$  to 40 and we check whether each geodesic has reached  $Z = 10$  within this time frame. If they haven't yet they most likely never will and can therefore be left out.

Second of all if  $r \leq r_s$  in any part of the geodesic, the geodesic will be removed. That is because the geodesic falls within the Schwarzschild radius if this condition is met, meaning It is sucked into the black hole and disappears completely.

Finally if a geodesic is mapped outside of the  $X, Y$  interval it originated from, it should be removed as well. That is because the light ray would be mapped outside of the output image  $X, Y$  interval meaning it wouldn't be visible in the transformed image.

Implementing these conditions in Python was one of the most time-consuming processes of the entire thesis. The problem was the fact that the pre-built Python solver returned a list of each involved variable after it was done solving the system of differential equations. There was no possibility of checking whether specific variables met the prescribed conditions during the computing process. I saw no other options than to use an entirely different pre-built Python solver which did allow intermediate checking. I eventually found the solver *ivp*, which did meet this requirement. Still it was difficult to check for these events but eventually I was able to implement the 3 described conditions to this new solver. If we now look at the geodesics left at  $t = 40$  given the required conditions, we find the following plot.

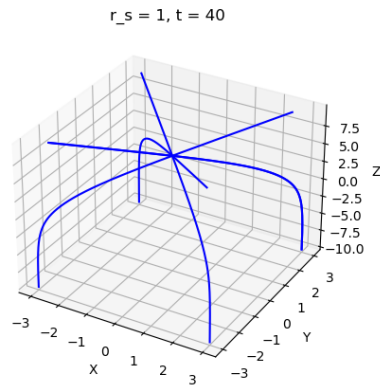


Figure 19: We set  $r_s = 1$  and  $t_{\text{end}} = 40$ . We see the (only) 4 geodesics left after reaching  $t_{\text{end}}$  given the required geodesic conditions.

Now compare this plot to the same scenario without restricted conditions.

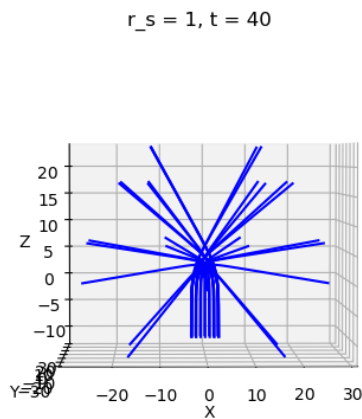


Figure 20: We set  $r_s = 1$  and  $t_{\text{end}} = 40$ . We see the geodesics left after reaching  $t_{\text{end}}$  without any required geodesic conditions.

The vast majority of the light rays vanished when we implemented the conditions. In fact only 4 geodesics of the 36 remain. This may seem very drastic but note that an  $r_s$  value of 1 is really high. This means a lot of geodesics fall within the Schwarzschild radius, get mapped outside the projected starting plane or are bent back to the starting plane and therefore are left out. I explicitly choose this higher  $r_s$  value to emphasize the differences between no geodesic restrictions and hard geodesic restrictions. Usually

we'll be dealing with smaller  $r_s$  values and the differences are therefore less significant. Besides we'll increase the field size we are working in meaning there are a lot more light rays that aren't bent as much since they are further away from the origin.

The scatter plot proved very uninteresting for the Minkowski metric but not for the Schwarzschild metric. This gives a very clear visualization of how the field is manipulated.

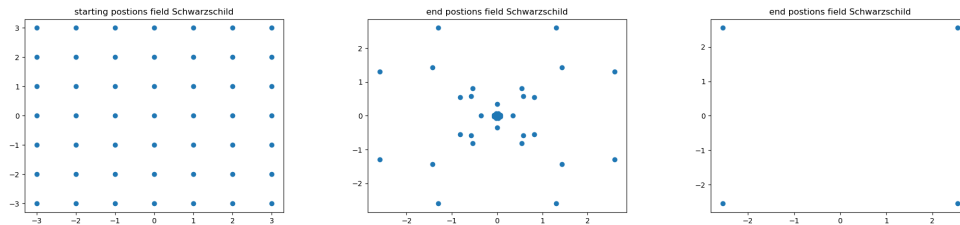


Figure 21: Left: the starting positions of all the geodesics in the 6x6 field, middle: the end positions of all the geodesics in the 6x6 field without geodesic restrictions ( $r_s = 1$ ), right: the end positions of all the geodesics in the 6x6 field with geodesic restrictions ( $r_s = 1$ ).

Clearly there's a massive manipulation of the original starting points in the middle plot, which corresponds to figure 20. The right plot corresponds to figure 19 where there's only 4 geodesics left. The scatter plot does lack information about which starting points are mapped to the specific end positions. In the right image for instance, we know that the geodesic rays actually intersect each other and change position completely as we can see in figure 19, which is not visible in the scatter plot however. Nonetheless the scatter plot does prove to be quite useful. In the middle image it may appear like there's an ending point precisely at  $X = Y = 0$ , but that is not the case. This becomes clear if we zoom in a bit.

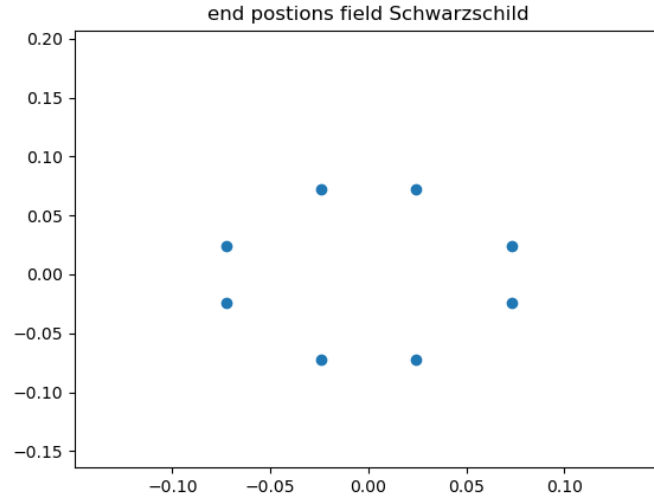


Figure 22: Zoomed in scatter plot of the end positions of all the geodesics in the 6x6 field.

## 7.8 Transforming images

This section is basically what the entire thesis has been building up to: the visualisation of the output image from the perspective of the observer. We are using all the knowledge we have gained in all the previous sections combined.

We'll start with the differences between the Schwarzschild image constructor and the Minkowski image constructor. First of all the Minkowski image constructor also worked with non-square images where the  $x$ -interval and  $y$ -interval were not equal. In the Schwarzschild metric each image has to be a perfect square, or else the black hole will be stretched out in the longer width or height. We want to crop each image in such a way that we have the biggest possible square in the middle of the original image. In order to do so we first of all determine the height and width of the original image in pixels. Then we take the smaller of the two and set the cropped width and cropped height equal to that value. We check the difference between the cropped width and original width, divide this by 2 and denote this value as start width. We do the same for the height, i.e. we determine the difference between the cropped height and original height, divide this by 2 and denote this value as start height. We then crop the image such that the height runs from start height to start height + cropped height and the width runs from start width to start width + new width. With this method we always have a square in the middle of the image.

The second difference between Schwarzschild imaging and Minkowski imaging is the size of the plane where the original image is located. In the Minkowski space the width

of the image in pixels corresponded to the  $x$ -interval and the height of the image corresponded to the  $y$ -interval translated such that the origin is placed in the middle. For example, if we had an input image of 100x100 the interval occupied by the image would be  $[-50, 50] \times [-50, 50]$ . And if we had an image of 200x200 the interval occupied by the image would be  $[-100, 100] \times [-100, 100]$ , etc. Since Minkowski space consisted of straight lines, it did not matter where the geodesic would begin with regards to the origin. When we are dealing with the Schwarzschild metric this is no longer the case. Geodesics close to the origin will be extremely bent whereas geodesics far removed from the origin will be close to straight lines. Applying the Minkowski approach would mean that if we would double the number of pixels, the ratio: surface contained within the Schwarzschild radius to total image surface, would halve. This is clearly not what we want. Just because the resolution increases shouldn't mean that the Schwarzschild radius contained surface should decrease. We want this ratio to remain the same no matter the resolution of the original image. A suitable way to solve this issue is to map every image, no matter the resolution, to a specified interval. We choose this interval to be  $[-10, 10] \times [10, 10]$ . We iterate over each column from left to right and then continue to the next row. Each pixel's position will be expressed by its column index:  $x$  and row index:  $y$ . This row and column index will be transposed in the following way to make sure they are mapped to  $[-10, 10] \times [10, 10]$ :  $x_{\text{start}} = -10 + 20 \cdot (x/x_{\text{size}})$ ,  $y_{\text{start}} = 10 - 20 \cdot (y/y_{\text{size}})$ . This transposition implies we start at the top left:  $(-10, 10)$ , and end at bottom right:  $(10, -10)$ . The  $x_{\text{start}}$  and  $y_{\text{start}}$  will be fed into geodesic constructor. After the geodesic constructor determined the  $x_{\text{end}}$  and  $y_{\text{end}}$  positions, they are transposed back to the original pixel row and column by the inverse formula:  $x_{\text{end}} = (x_{\text{end}} + 10) \cdot x_{\text{size}}/20$ ,  $y_{\text{end}} = (y_{\text{end}} - 10) \cdot y_{\text{size}}/-20$ . The events in the solver make sure that all conditions are met.

We are now able to transform an image in the Schwarzschild metric, similarly to how we this was done in the Minkowski metric. This results in the following image.



Figure 23: Left: the 100x100 input image in Schwarzschild metric, right: the 100x100 output image in the Schwarzschild metric.

Finally we are able to visualise the output with respect to the perspective of the observer!

Notice how we have a black circle in the middle of the image. This circle is caused by all the geodesics which enter within the Schwarzschild radius and therefore vanish. Since the output image is firstly completely blacked-out, the area within the schwarzschild radius is completely black. The fact that It is black makes sense since no light rays can escape and there's therefore an absence of light: darkness.

We also notice that there's a ring surrounding the black hole where massive image distortion takes place. As a matter of fact part of the image is actually turned upside-down in this ring. This may seem very strange, but if we take a look at the light trajectories from figure 20, we see that close to the Schwarzschild radius the curvature is so extreme that light rays actually intersect and cross and therefore turn parts of the image upside down.

Just outside the ring we see a lot of curvature as well, but the original image is still recognizable. The more we move to the edges, the more the curvature decreases. The most outward pixels experience almost no curvature whatsoever. This makes sense since the gravitational pull decreases as we move further away from the black hole.

We can visualise the transformation in a three-dimensional plot similar to figure 15. We plot the black hole with its corresponding Schwarzschild radius on scale in the the origin of the image as a black sphere. This results in the following plot.

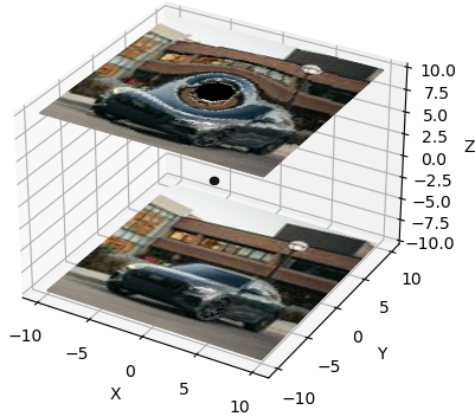


Figure 24: A three dimensional plot containing the original image at  $Z = -10$ , the black hole identified by its Schwarzschild radius in the origin and the distorted image at  $Z = 10$

The amount of distortion depends on the size of the Schwarzschild radius: the  $r_s$  value, and the distance of the observer relative to the black hole. We want to have an idea of how both factors influence the transformation of the original image.

To start off we determine how the image distortion relates to the  $r_s$  value. Clearly a higher  $r_s$  value will mean a higher amount of distortion, but just how much is unclear. I plotted the same image with 3 different  $r_s$  values to visualise the distortion. The  $Z_{\text{end}}$  is set to 10 as usual for all images.



Figure 25: Left: the output image given  $r_s = 0.2$ , middle: the output image given  $r_s = 0.4$ , right: the output image given  $r_s = 0.8$ .

We see that the surface within the black middle circle is directly proportional to the  $r_s$  value, meaning that if  $r_s$  doubles this surface doubles as well. This makes sense since

the Schwarzschild radius is doubled. More importantly as the  $r_s$  value increases the distortion around the outside of the ring increases as well. This amount of increased distortion outside of the ring seems directly proportional to the  $r_s$  value as well. Notice that the width of the ring remains the same for all  $r_s$  values.

To visualise the influence of the second distortion factor: the distance of the observer to the black hole, we will plot the same image with 3 different observer distances.



Figure 26: Left: the output image given  $Z_{\text{end}} = 5$ , middle: the output image given  $Z_{\text{end}} = 10$  right: the output image given  $Z_{\text{end}} = 20$ .

Note that when the observer is further away from the black hole, the curved light rays will diverge further meaning that the original image will be more distorted. For me this seemed counter-intuitive since I expected there to be more curvature when the observer is closer to the black hole than when the observer is further, but this is not the case. The plots clearly visualise this notion. We see that the black circle increases as the observer distance increases, but in no way directly proportional to each other. That is because the differences in the size of the surface of the black-circle doesn't change that much at all between the images. The curvature outside of the ring does seem to be directly proportional to the distance to the origin. Actually the curvature outside the ring is almost indistinguishable from the curvature seen in figure 25, which to me is very peculiar but interesting. Notice that the width of the ring seems directly proportional to  $r_s$  as well which is the main difference with respect to image 25.

Now that we are able to construct the image the observer sees as well as manipulate the parameters to create a black hole to our liking, we can basically construct any image transformation we want. I updated the code so that higher resolution images work as well. The next section of the thesis will be solely dedicated to the constructing of the transformed images.



## 8 Created images

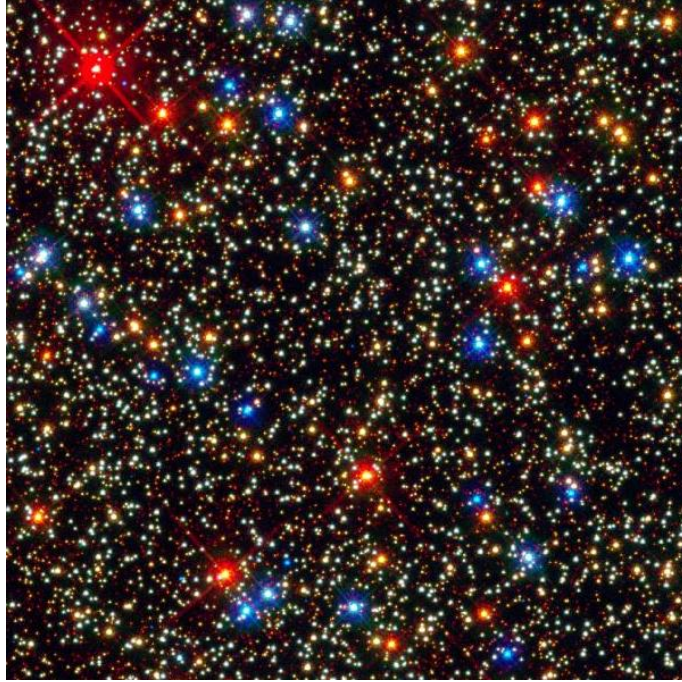


Figure 27: This image filled with distant stars, consists of 600 pixels in width and 600 pixels in height.

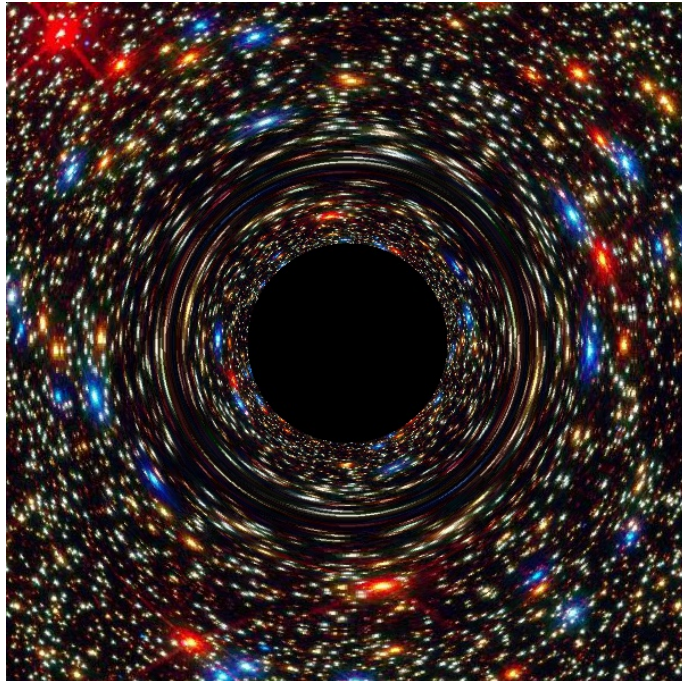


Figure 28: The  $r_s$  value is set to 0.5 and the  $Z_{\text{end}}$  distance the observer has to the black hole is 20.



Figure 29: This image of a nebula and some distant stars, consists of 479 pixels in width and 479 pixels in height.

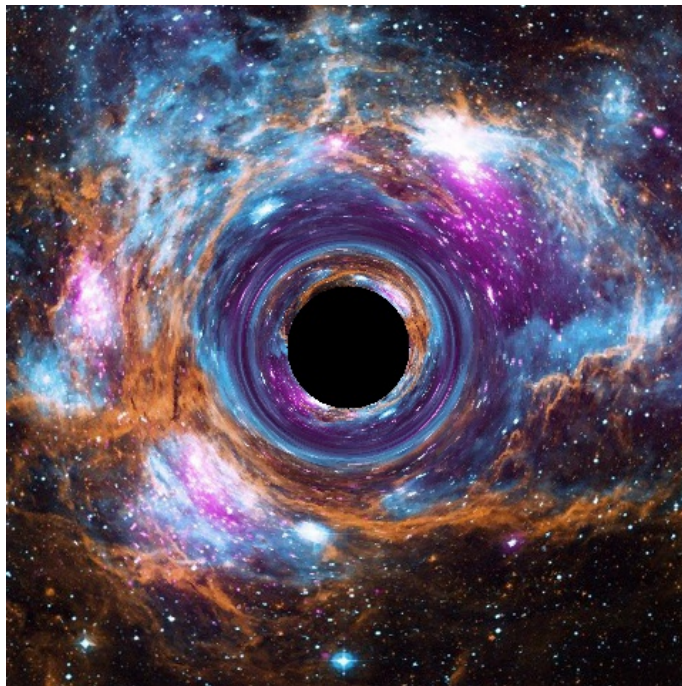


Figure 30: The  $r_s$  value is set to 0.4 and the  $Z_{\text{end}}$  distance the observer has to the black hole is 10.



Figure 31: This image containing a nebula and some distant stars, consists of 747 pixels in width and 747 pixels in height.

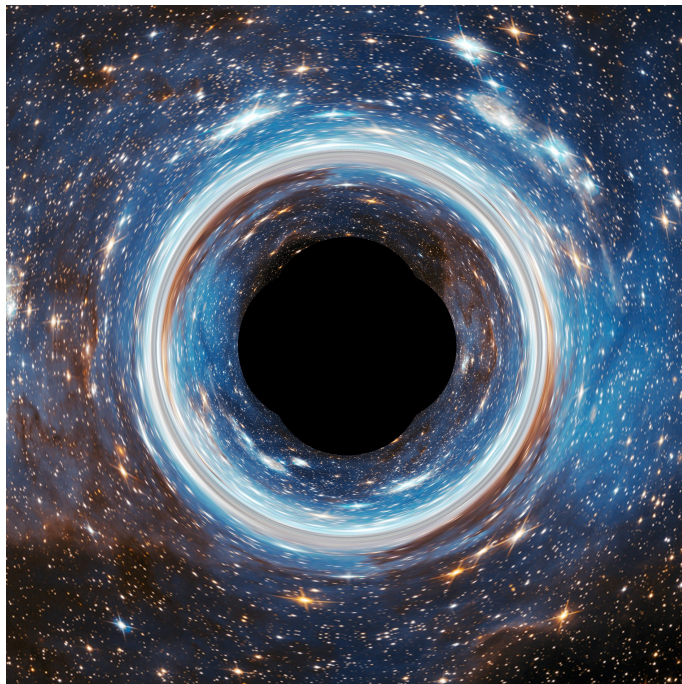


Figure 32: The  $r_s$  value is set to 0.65 and the  $Z_{\text{end}}$  distance the observer has to the black hole is 20.



Figure 33: This image containing a nebula and some distant stars, consists of 884 pixels in width and 884 pixels in height.

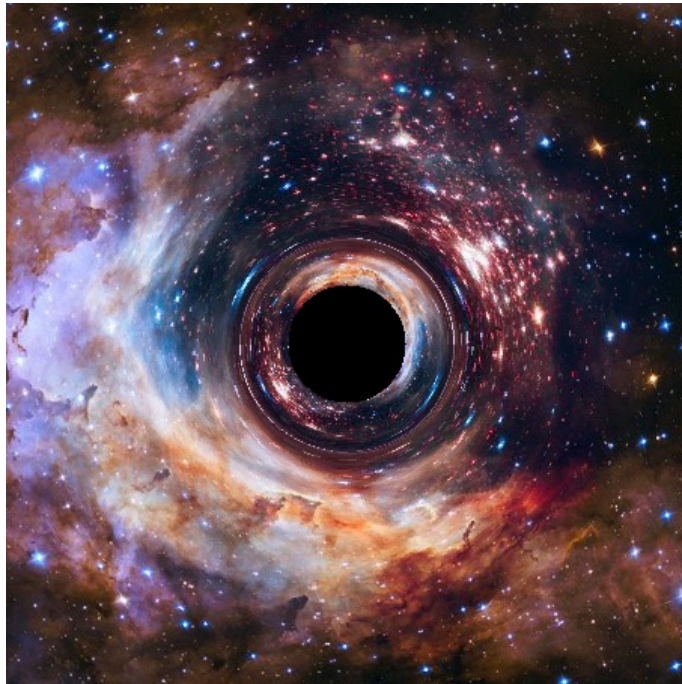


Figure 34: The  $r_s$  value is set to 0.4 and the  $Z_{\text{end}}$  distance the observer has to the black hole is 10.



Figure 35: This image containing a nebula and some distant stars, consists of 340 pixels in width and 340 pixels in height.

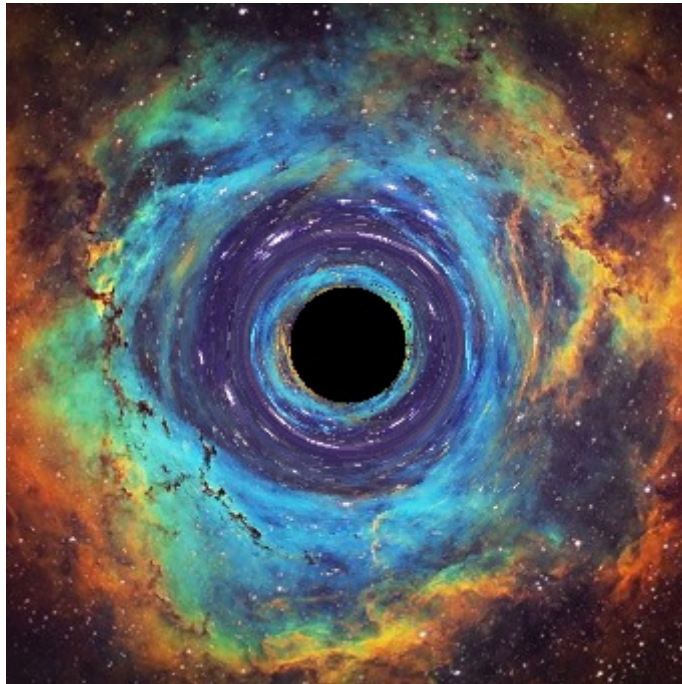


Figure 36: The  $r_s$  value is set to 0.3 and the  $Z_{\text{end}}$  distance the observer has to the black hole is 30.



Figure 37: This image taken by the Hubble telescope, consists of 1438 pixels in width and 1438 pixels in height.



Figure 38: The  $r_s$  value is set to 0.4 and the  $Z_{\text{end}}$  distance the observer has to the black hole is 10.



Figure 39: This image taken of a nebula, consists of 413 pixels in width and 413 pixels in height.

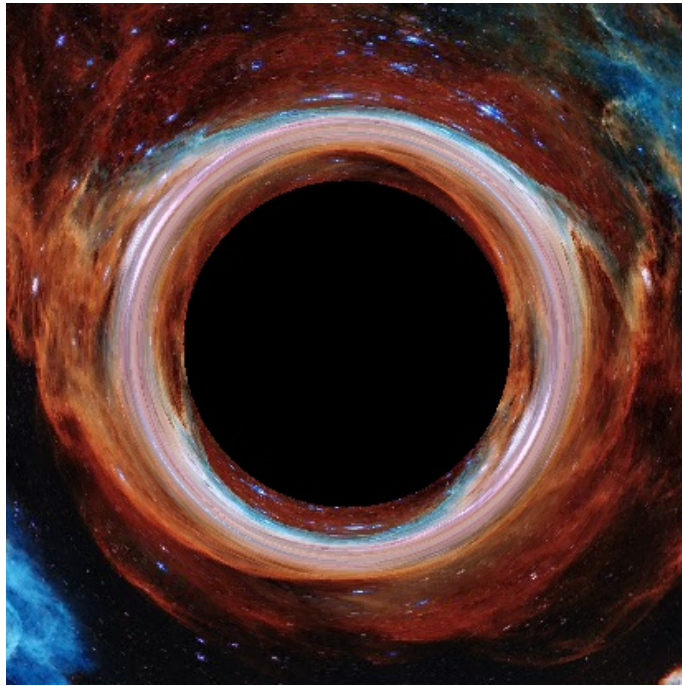


Figure 40: The  $r_s$  value is set to 0.8 and the  $Z_{\text{end}}$  distance the observer has to the black hole is 20.



Figure 41: This image taken of a nebula, consists of 898 pixels in width and 898 pixels in height.

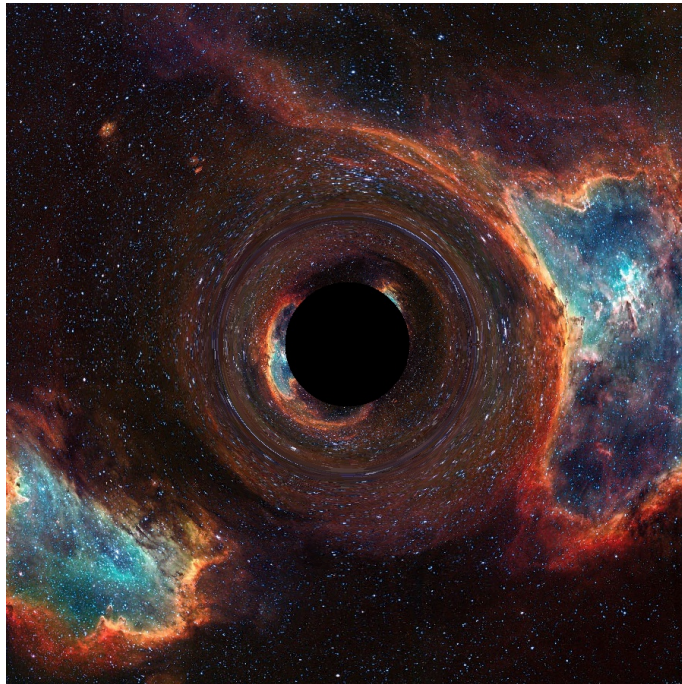


Figure 42: The  $r_s$  value is set to 0.3 and the  $Z_{\text{end}}$  distance the observer has to the black hole is 20.

## 9 Conclusion

Let's go all the way back to the Introduction where we constructed the end goal of our thesis: simulating and visualising the distortion of the image caused by the gravitational field of a black hole. As can be seen the goal actually consists of two individual though overlapping parts, namely the simulation and visualisation. We proceed by reflecting on the first part, the simulation. Though the simulation foundation is already laid in section (5), it is not until section (7) that we actually started simulation in the black hole metric. In this section we simulated light ray paths by means of a few consecutive steps. First of all we applied the geodesic equation to this metric and solved the resulting system of differential equations. Secondly we defined suitable initial positions and initial velocities. Finally we applied further conditions to remove those light rays that play no role in the projected image. Once we took these steps and thus have the trajectories of the light rays we constructed the projected image, the image which was altered by the gravitational field of the black hole. By validating our results we concluded that we have indeed successfully completed the first part of our goal, the simulation.

We then continue by reflecting on the second part of our goal (and with that the entire goal), the visualisation. The visualisation is actually only a small extension of the simulation and is discussed in the last part of section (7). Here we had translated all the results from the simulation in such a way that the projected image was actually visible to us. This allowed us to compare the projected image to the original and with that determine their similarities and differences. Section (8) is specifically dedicated to showcasing the projected image in comparison to the original image of several space images. This meant we had completed the second part of our goal as well, the visualisation. With that we have successfully completed our (total) goal.

Besides the goal it is worth reflecting on all the acquired knowledge we have gained throughout this thesis. In the Introduction we briefly discussed the notions of a black hole and of gravitational lensing which form the absolute main concepts of the thesis. In section (2) we extend our view and discussed the relevant Physics theory that forms the framework of the thesis. All of this was new to me as a mathematics student, but therefore all the more interesting. After forming a step by step plan of approach in section (3), we start with the Mathematics of the thesis in the following sections. In section (4) we are introduced to new mathematical concepts such as extrinsic geometry, the Christoffel symbols, the second fundamental form, the metric tensor, etc. and to new forms of notation such as the Einstein's summation convention. Here we form a general understanding of these mathematical concepts but in the following section, section (5) we are immediately applying all of them. Though I had some familiarity with spherical coordinates, dot products and calculating derivatives most of the mathematics in this section was new to me. In this section we apply the geodesic equation for the first time by substituting the calculated Christoffel symbols. In section (6) and even more so in section (7), the metric tensor significantly increased in size and therefore there are a lot more Christoffel symbols to deal with which created a greater challenge. All the

mathematics involved falls within the category of differential geometry with which I had no previous experience with whatsoever. Especially at the start of my thesis I was struggling a lot with the notation and mathematical concepts of differential geometry. By being thrown in the deep, meaning applying these concepts to actual metric spaces meant I made a lot of mistakes however therefore learned a whole lot.

Python code: [https://github.com/WouterKleynen/BEP\\_software](https://github.com/WouterKleynen/BEP_software)

## References

- [1] Ludvigsen, Malcolm (1999), *General Relativity: A Geometrical Approach*, p. 88
- [2] Carroll, Sean (2003), *Spacetime and Geometry: An Introduction to General Relativity*
- [3] D'inverno, Ray (1992), *Introducing Einstein's Relativity*
- [4] Videos added by eigenchris (2018), *Tensor Calculus*, YouTube video series. Available at <https://www.youtube.com/watch?v=kGXr1SF3WmA&list=PLJHszsWbB6hpk5h81SfBkVrpjsqvUGTCx>
- [5] NASA, *Black Holes*: <https://science.nasa.gov/astrophysics/focus-areas/blackholes>
- [6] space.com, *What Exactly Is a Black Hole Event Horizon?* : <https://www.space.com/blackholes-event-horizon-explained.html>
- [7] space.com, *What happens at the center of a black hole?* : <https://www.space.com/what-happens-blackhole-center>
- [8] Isaac Newton (Encyclopædia Britannica), *The Mathematical Principles of Natural Philosophy* : <https://www.britannica.com/topic/The-Mathematical-Principles-of-Natural-Philosophy>
- [9] Albert Einstein, *Zur Elektrodynamik bewegter Körper*, *Annalen der Physik* 17: 891 : [https://web.archive.org/web/20050220050316/http://www.pro-physik.de/Phy/pdfs/ger\\_890\\_921.pdf](https://web.archive.org/web/20050220050316/http://www.pro-physik.de/Phy/pdfs/ger_890_921.pdf)
- [10] Karl Schwarzschild, *Über das Gravitationsfeld eines Massenpunktes nach der Einsteinschen Theorie*: [https://de.wikisource.org/wiki/Gravitationsfeld\\_einer\\_Kugel\\_aus\\_inkompressibler\\_Fl%C3%BCssigkeit](https://de.wikisource.org/wiki/Gravitationsfeld_einer_Kugel_aus_inkompressibler_Fl%C3%BCssigkeit)
- [11] forbes.com, *Ask Ethan: What Is Spacetime?* : <https://www.forbes.com/sites/startswithabang/2017/01/28/ask-ethan-what-is-spacetime/?sh=1782456f50bd>
- [12] Australian Academy of Science, *Gravitational lensing* : <https://www.science.org.au/curious/space-time/gravitational-lensing>
- [13] Science alert, *What Is The General Theory of Relativity?* : <https://www.sciencealert.com/general-relativity>
- [14] caranddriver.com, *Audi Q8 image* : <https://www.caranddriver.com/photos/g25585409/2019-audi-q8-suv-by-the-numbers-gallery/>
- [15] taringa.net, *Space image* : [https://www.taringa.net/+imagenes/espectaculares-imagenes-del-telescopio-hubble\\_12yln7](https://www.taringa.net/+imagenes/espectaculares-imagenes-del-telescopio-hubble_12yln7)

- [16] stock.adobe.com, *Space image* : [https://stock.adobe.com/nl/186546012?as\\_campaign=TinEye&as\\_content=tineye\\_match&epi1=186546012&tduid=141aed69e105de4de184d9eca0fc1b0a&as\\_channel=affiliate&as\\_campclass=redirect&as\\_source=arvato](https://stock.adobe.com/nl/186546012?as_campaign=TinEye&as_content=tineye_match&epi1=186546012&tduid=141aed69e105de4de184d9eca0fc1b0a&as_channel=affiliate&as_campclass=redirect&as_source=arvato)
- [17] stock.adobe.com, *Space image* : [https://stock.adobe.com/347427413?as\\_campaign=TinEye&as\\_content=tineye\\_match&epi1=347427413&tduid=141aed69e105de4de184d9eca0fc1b0a&as\\_channel=affiliate&as\\_campclass=redirect&as\\_source=arvato](https://stock.adobe.com/347427413?as_campaign=TinEye&as_content=tineye_match&epi1=347427413&tduid=141aed69e105de4de184d9eca0fc1b0a&as_channel=affiliate&as_campclass=redirect&as_source=arvato)
- [18] stock.adobe.com, *Space image* : [https://stock.adobe.com/254856938?as\\_campaign=TinEye&as\\_content=tineye\\_match&epi1=254856938&tduid=141aed69e105de4de184d9eca0fc1b0a&as\\_channel=affiliate&as\\_campclass=redirect&as\\_source=arvato](https://stock.adobe.com/254856938?as_campaign=TinEye&as_content=tineye_match&epi1=254856938&tduid=141aed69e105de4de184d9eca0fc1b0a&as_channel=affiliate&as_campclass=redirect&as_source=arvato)
- [19] rawpixel.com, *Space image* : <https://www.rawpixel.com/image/440211/free-photo-image-nebula-nasa-hubble>
- [20] BBC.com, *Space image* : <https://www.bbc.com/news/science-environment-57885865?xtor=AL-72-%5Bpartner%5D-%5Byahoo.north.america%5D-%5Blink%5D-%5Bnews%5D-%5Bbizdev%5D-%5Bisapi%5D>
- [21] stock.adobe.com, *Space image* : [https://stock.adobe.com/101426449?as\\_campaign=TinEye&as\\_content=tineye\\_match&epi1=101426449&tduid=141aed69e105de4de184d9eca0fc1b0a&as\\_channel=affiliate&as\\_campclass=redirect&as\\_source=arvato](https://stock.adobe.com/101426449?as_campaign=TinEye&as_content=tineye_match&epi1=101426449&tduid=141aed69e105de4de184d9eca0fc1b0a&as_channel=affiliate&as_campclass=redirect&as_source=arvato)
- [22] Reddit, *Space image* : <https://www.reddit.com/user/RayKam?sort=top>
- [23] fileformat.info, *Unicode Character 'FULLWIDTH QUESTION MARK' (U+FF1F)* : <https://www.fileformat.info/info/unicode/char/ff1f/index.htm>
- [24] Vincent van Gogh, *A Starry Night*